Neurobiology of Disease xxx (xxxx) xxxx

Contents lists available at ScienceDirect

Neurobiology of Disease

journal homepage: www.elsevier.com/locate/ynbdi

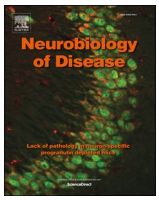

Review

Positron emission tomography studies of organophosphate chemical threats and oxime countermeasures

Charles M. Thompson[a,*], John M. Gerdes[a], Henry F. VanBrocklin[b]

[a] Department of Biomedical and Pharmaceutical Sciences, University of Montana, Missoula, MT 59812, USA
[b] Department of Radiology and Biomedical Imaging, University of California, San Francisco 185 Berry St. Suite 350, San Francisco, CA 94107, USA

ARTICLE INFO

Keywords:
Positron emission tomography (PET)
Imaging
Biodistribution
Pharmacokinetics/toxicokinetics
Pharmacodynamics/toxicodynamics
Organophosphate/organophosphorus
Oxime
Fluorine-18
Carbon-11
Acetylcholinesterase
Inhibition
Reactivation
Aging

ABSTRACT

There is a unique *in vivo* interplay involving the mechanism of inactivation of acetylcholinesterase (AChE) by toxic organophosphorus (OP) compounds and the restoration of AChE activity by oxime antidotes. OP compounds form covalent adducts to this critical enzyme target and oximes are introduced to directly displace the OP from AChE. For the most part, the *in vivo* inactivation of AChE leading to neurotoxicity and antidote-based therapeutic reversal of this mechanism are well understood, however, these molecular-level events have not been evaluated by dynamic imaging in living systems at millimeter resolution. A deeper understanding of these critically, time-dependent mechanisms is needed to develop new countermeasures. To address this void and to help accelerate the development of new countermeasures, positron-emission tomography (PET) has been investigated as a unique opportunity to create platform technologies to directly examine the interdependent toxicokinetic/pharmacokinetic and toxicodynamic/pharmacodynamic features of OPs and oximes in real time within live animals. This review will cover two first-in-class PET tracers representing an OP and an oxime antidote, including their preparation, requisite pharmacologic investigations, mechanistic interpretations, biodistribution and imaging.

1. Introduction

Although a continued threat to civilians exists from government/military use of toxic organophosphorus (OP) chemical warfare agents (CWAs), a mounting and equally troubling concern is that highly lethal forms of OPs are relatively accessible or can be prepared from inexpensive precursors. It is a solemn realization, therefore, that toxic OPs can be synthesized in a small space and are a more practical weapon to a shadow organization than biological or radioactive agents. Whether prepared or acquired illegally, the potential remains that rogue groups or nations will deploy OPs in actions against civilians ranging from large urban centers to targeted individuals (Chai et al., 2017; Holstege et al., 1997; John et al., 2018; Okumura et al., 2005a). However, the availability of toxic substances is only one concern. OPs are among the most feared chemical weapons due a combination of factors. Foremost, OPs are very toxic, for example, an oral exposure of just 0.5 mg VX is enough to kill a 75 kg human and in non-lethal cases cause seizure that can progress to status epilepticus (Chai et al., 2017). Even a single, low-level exposure to an OP can cause serious neurologic problems. Second, OPs are remarkably fast acting with symptoms of neurotoxicity occurring within one minute of exposure. This is due to the fact that OPs block an essential, ultra-fast neurotransmitter-processing enzyme in the central nervous system (CNS) called acetylcholinesterase (AChE).

The rapid onset of toxicity and array of symptoms from OP exposures presents numerous challenges for first responders who must identify the exposure type and administer standard of care therapeutics (Deshpande et al., 2016; McCarren et al., 2018; Niquet et al., 2017a; Niquet et al., 2017b; Skovira et al., 2010). Thus, exposure to OPs presents a multi-tiered challenge to address a complex toxidrome that is dose- and time-sensitive. As researchers better characterize toxic pathways associated with OP exposures and formulate possible pharmacotherapies, it became clear that the field lacked a platform technology – a routine or standardized approach to understand the rapid toxicokinetics and to interrogate new and existing countermeasures. A well-defined, consistent approach to acquire and assess dynamic, *in vivo* molecular-level events at the origin of exposure would more rapidly advance new and existing therapeutics.

* Corresponding author at: Department of Biomedical and Pharmaceutical Sciences, College of Health Professions and Biomedical Sciences, University of Montana, Missoula, MT 59812, USA.
E-mail address: charles.thompson@umontana.edu (C.M. Thompson).

https://doi.org/10.1016/j.nbd.2019.04.011
Received 16 November 2018; Received in revised form 28 March 2019; Accepted 19 April 2019

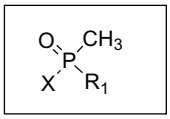

Chemical Warfare Agents
VX: R_1 = OCH_2CH_3, X = $SCH_2CH_2N(iPr)_2$
Sarin: R_1 = $OCH(CH_3)_2$, X = F
Cyclosarin: R_1 = OC_6H_{11}, X = F
Soman: R_1 = $OCH(CH_3)C(CH_3)_3$, X = F
Tabun: R_1 = $N(CH_3)_2$, X = CN

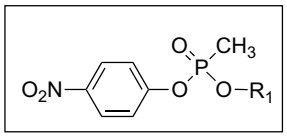

Chemical Agent Surrogates
VX surrogate: R_1 = CH_2CH_3
F-VX surrogate: R_1 = CH_2CH_2F
Sarin surrogate: R_1 = $CH(CH_3)_2$
F-Sarin surrogate: R_1 = $CH(CH_2F)(CH_3)$

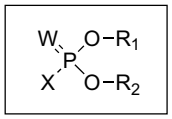

Insecticides
Parathion: W = S, R_1/R_2 = Et, X = p-nitrophenoxy (PNP)
Paraoxon: W = O, R_1/R_2 = Et, X = p-nitrophenoxy (PNP)
Chlorpyrifos: W = S, R_1/R_2 = Et, X = O-(3,5,6-trichloropyridinyl)
Malathion: W = S, R_1/R_2 = Et, X = $SCH(CO_2Et)CH_2CO_2Et$
Phosphorylating Agent
DFP: W = O, R_1 = iPr, X = F

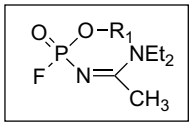

Novichok
A-232: R_1 = CH_3
A-234: R_1 = CH_2CH_3

Fig. 1. Examples of organophosphorus structures representing CWAs, insecticides, novichok, and chemical agent surrogates.

2. Organophosphorus compounds

2.1. Structure of toxic organophosphorus compounds

Toxic organophosphorus (OP) compounds include the chemical warfare agents (CWAs) such as the G-agents (*e.g.*, sarin, soman, cyclosarin, tabun) and V-agents (VX, VR), the novichoks (*e.g.*, A-232 and A-234), the serine protease inhibitor diisopropyl fluorophosphate (DFP), and certain insecticides like parathion and paraoxon among others (Fig. 1). Most toxic OP compounds are pentavalent structures bearing three single-bonded groups and a pi-bond (P═O or P═S) (Fig. 1). CWAs are distinguished by a methyl to phosphorus bond (phosphonate), phosphoryl (P═O), phosphoester (P-OR) and bear a leaving group such as fluorine (G-agents) or substituted thiolester (P-SR; V-agents). OP insecticides typically have two identical phosphorus ester groups usually P-OMe or P-OEt, a thiophosphoryl (P═S) and usually an O-aryl leaving group. The thiophosphoryl imparts greatly reduced reactivity as compared to P═O, and O-aryl leaving groups are less reactive and volatile than fluorine leading to a combination of properties that confers a greater margin of safety to the use of OP insecticides.

The key chemical transformation that renders OP insecticides toxic is the conversion of the relatively unreactive thiophosphoryl (P═S) moiety into the corresponding oxon (P═O). The process occurs readily *in vivo* in principle converted or 'activating' the insecticide into the oxon form (P═O) and increasing the reactivity toward AChE by about 1000-fold. DFP and the novichoks contain the P═O and the fluorine leaving group, and like the CWAs require no oxidative activation. CWAs differ from the other OPs in that they contain a carbon-phosphorus (phosphonate) bond.

2.2. Mechanism of acetylcholinesterase inhibition

The triggering event in OP toxicity is the inhibition of AChE (Scheme 1). When AChE is inactivated, it can no longer hydrolyze the neurotransmitter acetylcholine (ACh): a process that if unabated causes synaptic concentrations of ACh to rise to toxic levels stimulating autonomic receptors and depolarizing block of neuromuscular junction receptors on the post-synaptic neuron (Fukuto, 1990a; Gallo and Lawryk, 1991; Stine and Brown, 1996; Sultatos, 1994; Taylor, 2018). The mechanism of inhibition is conserved for most reactive OP compounds and affords OP-AChE adducts that for CWAs bearing R^1 = Me vary only in the alkyl substituent R^2 (Scheme 1). This difference in alkoxyl group dictates the rate and extent of inhibition and post-inhibition mechanism (*vide infra*). Paraoxon, the oxidized form of parathion, affords a diethoxyphosphoryl adduct of AChE (R^1 = OEt, R^2 = Et). Butyrylcholinesterase (BChE) and other serine hydrolases can also be inactivated by OPs (Casida and Quistad, 2005) but most are not linked to the neurologic sequelae.

OP inhibition of AChE forms an OP-AChE adduct that is far more stable than the acylated adduct formed from the natural substrate ACh or the carbamoylated version formed from carbamate inhibitors (*e.g.*, physostigmine). Carbamoylated AChE adducts are somewhat labile and the enzyme activity can be restored in minutes by reaction with water whereas this 'spontaneous reactivation' process can take hours to days in the case of OP-AChE adducts (Scheme 1; water). For phosphylated AChE, spontaneous reactivation is facilitated when the alkoxy groups attached to phosphorus are small (*e.g.*, R^2 = Me, Et). When spontaneous reactivation is slow or impeded, sustained AChE inhibition occurs and accounts for the neurotoxic action (Taylor, 2018). Although the mechanism of AChE inhibition by OPs forms OP-AChE adducts, post-inhibitory processes are not limited to just spontaneous reactivation, and another process termed 'aging' can occur.

2.3. Reactivation and aging of OP-AChE adducts: oxime antidotes

Toxic OP exposures are treated with a standard of care (SOC) that includes a cholinesterase reactivator (an oxime), a muscarinic receptor antagonist (atropine), and an antiseizure agent (midazolam, diazepam) (Ohbu et al., 1997; Okumura et al., 1996) along with supportive care. The role of the oxime is specific to the mechanism of OP inhibition and restores AChE activity by displacing the OP moiety from the active site serine (Scheme 1). The process is greatly accelerated compared to spontaneous reactivation due to the affinity of cationic oximes for AChE and the oxime nucleophilicity. The clinically approved oximes include 2-PAM (US), HI-6 (Canada), and obidoxime or HI-6 (European Union). Although there is clear therapeutic value in the administration of oximes, none of those clinically-approved readily enter brain (Ahn et al., 2011; Shih et al., 2010a; Shih et al., 2010b) in large quantities due to their cation charge(s), and concentrates oximes in peripheral tissues. Oxime reactivators are also short acting with a rapid plasma

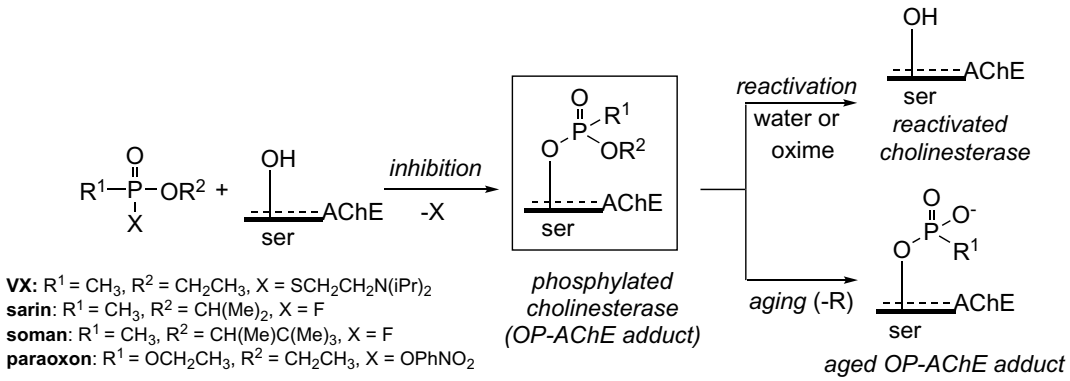

Scheme 1. Inhibition of AChE by OPs and the possible post-inhibition processes: reactivation and aging.

half-life of ~1–2 h (Jovanovic, 1989) typically requiring repetitive dosing. These combined factors can limit oxime reactivation of OP-modified AChE in the CNS. Further complicating oxime efficacy is the wide variation in the response of OP-AChE adducts to nucleophilic oximes with some OP-AChE adducts readily reactivated and some fully refractory to oxime therapeutic action. Without oxime intervention, prolonged blockade of AChE occurs and can lead to long-term neurologic symptoms as reported among Tokyo sarin attack victims (Okumura et al., 2005a; Okumura et al., 2005b).

The reactivation mechanism of OP-modified AChE is conserved among the oxime antidotes in which the oxime oxyanion moiety (R-CH=NO$^-$) displaces the entire phosphorus group from the serine hydroxyl (Ashani et al., 1998; Berkman et al., 1993; Berman et al., 1995; Langenberg et al., 1988; Lanks and Seleznick, 1981; Lieske et al., 1980; Ryu et al., 1991; Wilson et al., 1992). Oximes work extremely well when the phosphorus group attached to serine contains small groups (Scheme 1; R^1, R^2 = Me, Et) and the oxime proficiency decreases as the size of the groups attached to phosphorus increase. For example, if the phosphorus moiety contains a highly branched ester group (Scheme 1; R^2 = iPr, *etc.*), it is more difficult for the nucleophilic oxime to approach the phosphorus to displace it from the serine. Moreover, certain OP-AChE adducts can become non-reactive toward oximes due to 'aging' in which the OP-AChE adduct forms a phosphorus oxyanion (Scheme 1). Aging arises when a phosphorus alkyl (R^2) group is cleaved from the OP-AChE complex (Barak et al., 1997; Elhanany et al., 2001; George et al., 2003; Lanks and Seleznick, 1981; Millard et al., 1999; Ordentlich et al., 1999; Wallace and Herzberg, 1988), and is more common when most readily when R^2 is highly branched. The resultant phosphoanion is refractory to oxime reactivation due to charge repulsion. Certain CWAs such as soman [R^2 = CH(Me)C(Me)$_3$] form OP-AChE adducts that undergo aging in minutes limiting the possibility of oxime reactivation.

To address the limitation in blood brain penetration by cationic oximes, hydrophobic analogs (Chambers et al., 2016a; Chambers et al., 2013; Chambers et al., 2016b; Chambers et al., 2016c) and neutral oximes (Bedford et al., 1986a; Bedford et al., 1986b; de Koning et al., 2011; Okuno et al., 2008; Radic et al., 2012; Sit et al., 2014; Sit et al., 2011) capable of penetrating the BBB have been investigated and show promise as useful alternatives to charged oximes. Recent attempts have also been made to reactivate aged AChE (Zhuang et al., 2018). With new structures being advanced as potential BBB-penetrating antidote therapeutics, investigators will need to accurately assess their clinical potential and could benefit from a dynamic functional assay in live vertebrates.

2.4. OP compounds: exposures and toxicity

Ps have a rich history as pest control agents in crop protection, flame retardants, plasticizers, and as highly useful reagents in the preparation of therapeutic drugs. Despite their importance and commercial success there remains a constant balancing act between utility and the public concerns connected with exposure to OP compounds. The principle reason for concern covered prior is that OP CWAs and OP insecticide oxons share chemical features (Fig. 1), high reactivity, and as covered prior, the same mechanism of toxic action including inactivation of AChE. It is alarming that significant quantities of OP reach target tissues in sufficient quantities to effectively disable AChE and cause neurotoxicity through many different exposure routes. Several physico-chemical properties expedite the enzyme-disabling event. Most neurotoxic OPs are very small molecules with molecular weight ~ 350 or less that are internalized rapidly upon exposure, experience facile passage and movement within the bloodstream, poorly bind plasma proteins (Black et al., 1999; Goncharov et al., 2017; Suganthi and Elango, 2017; Tarhoni et al., 2008), and penetrate cell (Bharate et al., 2010) and tissues *via* passive diffusion. Thus, OPs can cross membranes and accumulate to sufficient levels in brain where they can inactivate the target AChE but also peripheral AChE.

The cholinergic toxicity that results from either CWA or OP insecticide exposure has been reviewed (Ballantyne and Marrs, 1992; Barthold and Schier, 2005; Collombet, 2011; Gearhart et al., 1994; Taylor, 2018). Other non-cholinergic or possibly cholinergic-associated sequelae have been linked to OP exposures including ataxia, delayed neuropathy, pulmonary toxicity, genotoxicity, Parkinson's and vision loss (Aldridge and Nemery, 1984; Ames et al., 1995; Carlson and Ehrich, 2004; Dementi, 1994; Dyer et al., 2001; Gallo and Lawryk, 1991; Imamura and Gandy, 1988; Imamura and Hasegawa, 1984; Kamijima and Casida, 1999; Lotti and Moretto, 1999; Meinert et al., 2000; Moretto and Lotti, 1998; Richardson et al., 2013; Schuz et al., 2000; Sherman, 1996; Stephens et al., 1995; Stine and Brown, 1996). However, these toxicities are not connected through a common mechanism of inactivation nor a mutual target. Rather, much of the evidence connecting OPs to these non-cholinergic sequelae result from slower developing molecular events and/or chronic exposures to relatively weak anti-cholinesterases, which differ greatly in mode of action from the highly reactive OPs covered here (Fig. 1). Still, some non-AChE protein targets are modified by reactive OPs (Casida and Quistad, 2004b; Casida and Quistad, 2005);(Carlson and Ehrich, 2004; Casida and Quistad, 2004a; Casida and Quistad, 2005; Grigoryan et al., 2009; Grigoryan et al., 2008; Peeples et al., 2005; Tarhoni et al., 2008) although many do not affect the CNS.

3. Positron emission tomography

3.1. Positron emission tomography (PET) as a unique imaging tool

PET has become an increasingly valuable tool in research and clinical studies providing suitable levels of sensitivity over time while enabling entire live tissues and tissue regions, such as brain, to be

imaged over time and quantitatively analyzed using a relatively non-invasive procedure (Ametamey et al., 2008; Heiss and Herholz, 2006). PET tracers report on a dynamic, evolving biological process *in vivo* with the capacity to monitor distribution of small molecules into entire tissues or tissue regions, 'frame' specific time domains or snapshots of distribution, or acquire cumulative information in tissues or whole body over the lifetime of the tracer. The nature and unique capabilities of PET imaging exquisitely reports on tracer tissue and blood distributions and molecule-level interactions. PET studies are broadly interactive furnishing a deeper understanding of molecular events that inform and can lead to improved therapeutics. When it comes to measuring events at the molecular level for example enzyme/receptor interactions, pharmacokinetics, blood flow and pharmacologic characteristics, *in vivo* PET with parallel biodistribution profiling rates are among the most highly sensitive methods. What pertains most to OP exposures and toxicity is that the radioisotopes used in PET can be quantified at nanogram to picogram concentrations over time in live tissues, which is a key advantage over other imaging techniques given the microgram-level toxicity of OPs. This low level of detection is considered important for tracking the mechanism of action of OPs at sub-toxic (nanogram) levels. Often less appreciated is that the PET radioisotopes generated at a cyclotron facility decay quickly ($t_{½}$ ~ min to hr). In combination with PET tracer ultra-low sensitivity, the short half-lives are an advantage in that the live subject is rapidly cleared of radioisotope and in principle, available for additional tracer experiments where longitudinal studies are desired. However, short duration isotopes such as carbon-11 can present some challenges where biodistribution rates and binding mechanisms are slow. Still, a well-devised PET tracer even of limited half-life can be used to conduct both short- and long-range exposure studies on a single subject. For example, PET tracers can be introduced immediately following an OP exposure to interrogate changes in tissue levels, but can also be used to assess tissue changes from days to weeks post-exposure.

PET imaging and related studies offer a number of advantages to investigate OP threat agents and countermeasure therapies in live tissues. However, it is important to recognize that a significant body of previous *in vitro* and *in vivo* research, using traditional radiotracers (*e.g.*, tritium and carbon-14 radionuclides) pioneered this field (Firemark et al., 1964; Lenz et al., 1983; Little et al., 1986; Martin, 1985; Michel et al., 1967; Shapira et al., 1990; Viragh et al., 1999). These groundbreaking tracer investigations provided specific experimental insights as the biodistribution of select OPs or oximes to the PNS and CNS, the metabolism of OPs and oximes, and the effect of therapeutic oximes on the OP distribution and *vice versa*. In addition, these studies provided the important *in vitro* pharmacology, toxicology and biological benchmark data that can be used to validate the performance qualities of first-in-class PET tracers. Unique challenges to the present research are that unlike most PET studies of traditional drug binding, OP PET tracers covalently modify AChE as the target and conversely oxime antidotes lack a high-affinity pharmacologic target in the absence of an OP exposure. Even after an OP has modified AChE, the oxime does not truly 'bind' the target reacting only with OP-modified AChE.

Since OPs access brain within seconds to minutes regardless of the route of exposure or dose amount (ng to mg), positron emission tomography (PET) emerged as an ideal, dynamic quantitative methodology to first evaluate the rapid pharmacokinetic parameters of exposure and subsequently, to interrogate new and existing medical countermeasures in live subjects. However, present studies were undertaken with the understanding that the existing literature in PET research may not be fully applicable to OPs, and that a customized research approach may be needed to corroborate and confirm the *in vivo* pharmacokinetic and pharmacodynamic data thus obtained. Since OPs are considered toxicants and not drugs, the terms toxicokinetics and toxicodynamics are utilized for the OP tracer studies.(Welling, 1995) This review covers some recent advances using PET imaging and cognate biodistribution profiling to investigate OP mechanism of action and antidotes used to counteract toxic OP exposures. The preparation, development, optimization and *in vivo* analyses of new positron-labeled tracer analogs of OP threat agents and an oxime countermeasure are covered below.

3.2. PET imaging and biodistribution measures

It is widely appreciated that dynamic PET imaging is the preferred *in vivo* method for quantitative assessments of molecular level, biological-pharmacological events in live animals. PET studies targeting proteins and/or drug interactions have been used to extensively and successfully evaluate small molecule tracer tissue distribution profiles and tracer-target interactions in living tissue (Ametamey et al., 2008; Eckelman et al., 2006; Eckelman and Mathis, 2006a; Eckelman and Mathis, 2006b; Hesse et al., 2004; Laakso and Hietala, 2000; Laruelle et al., 2002). PET tracers (positron-labeled radioligands) employ a beta-emitter atom that after injection undergoes discrete kinetic compartmentalization processes resulting in three-dimensional (3D) reconstructed volumetric tissue images (Cunningham and Lammertsma, 1994; Innis et al., 2007; Laruelle et al., 2002; Laruelle et al., 2003) that are dependent on PET scanner resolution. Well-known strengths of PET include powerful quantitation of regional molecular level events (Frangioni, 2006), target protein populations (Frankle et al., 2004; Innis et al., 2007; Laruelle et al., 2003), tracer tissue distribution volume ratios (Ding and Fowler, 2005; Ding et al., 2006; Ding et al., 2005; Logan, 2000; Logan et al., 2005; Logan et al., 1990), and of relevance to this study target binding potentials for functional AChE (Blomqvist et al., 2001; Darvesh, 2013; Funaki et al., 2003; Heiss and Herholz, 2006; Hiraoka et al., 2009; Kikuchi et al., 2007; Kikuchi et al., 2010; Koeppe et al., 1999; Musachio et al., 2002; Pappata et al., 1996; Planas et al., 1994; Ryu et al., 2005; Shinotoh et al., 2004; Tavitian et al., 1993; Volkow et al., 2001). PET studies offer the advantage of *in vivo* dynamic imaging of tissues resulting in temporal measures occurring over the lifetime of the tracer. For some studies the imaging subject can be evaluated repeatedly (*e.g.*, on the same day or subsequent days) for longitudinal appraisal of temporal changes. Given the remarkable sensitivity of PET tracers, *in vivo* tissue events can be measured and followed with PET imaging, where biodistribution profiling further confirms tracer tissue fates. Tracers showing optimal *in vivo* profiles can be advanced into non-human primate imaging platforms that can be utilized by investigators to determine PK-PD profiles of new therapeutics or to satisfy FDA Animal Rule criteria (Borsook et al., 2013). Importantly, PET imaging-based platforms provide a means to establish proof of mechanism(s) of actions, which can be applied to the study of countermeasures acting at AChE and related targets.

3.3. Strategies and considerations for dynamic, in vivo assessments with covalent modifiers

One of the distinguishing characteristics of OP PET tracers is that they will covalently modify their target. Most drugs are translated into their corresponding PET tracer forms so that their target can be interrogated through traditional ligand binding interactions with known association/dissociation constants. In the case of OP tracers, dissociation rates are only relatable to the target AChE itself since a predictable long-term washout from AChE is not anticipated based on mechanism. Thus, an OP PET tracer can quantitatively report on available pools of AChE as the pharmacodynamic target. Since the target is covalently modified, tracer levels in AChE-rich tissues would be expected to rise initially and then undergo washout of free OP and OP metabolites to afford a steady state level of tracer corresponding to AChE-OP adduct. It is also possible that the AChE-OP tracer levels could decrease over the course of the experiment in cases where the OP undergoes the 'aging' process. In this instance, the OP-AChE adduct remains intact but the positron-labeled molecular component is lost along with the aged alkoxy group (lost to dealkylation).

Overall, OP tracers react with functionally-active AChE and then report on the resultant inactivated pool of enzyme. The extent and duration of AChE inhibition by OP PET tracers could be monitored within live animals in a time-dependent process, including inactivation by other OPs or reactivation by new and existing oxime antidotes. Although it is considered less consequential in the mechanism of toxicity, a covalent bond is also formed in the reactivation process when the oxime antidote reacts at the OP phosphorus atom to displace it from the AChE serine. However, OP-oximates are believed to be of transient lifetime due to Beckman-type elimination and/or hydrolysis (Ashani et al., 2003; Leader et al., 1999), and in the bloodstream where degrading enzymes are present such that the neurologic importance of OP-oximates is low.

3.4. PET radiotracers: carbon-11 and fluorine-18

The insertion or replacement of a radionuclide atom into a drug molecule is intended to 'label' or 'tag' the structure enabling *in vivo* tracking while retaining the PK properties and importantly, the specific PD action of the original drug. Among the PET radiotracers used in drug labeling, carbon-11 and fluorine-18 radionuclides are the most widely used. Carbon-11 is an important radionuclide because introduction into a drug molecule by replacement of a carbon-12 non-radioactive atom results in identical PK/PD characteristics (Antoni, 2015). However, the rapid half-life of carbon-11 (^{11}C, $t_{½}$ = 20 min) combined with the radiochemical transformation challenges of directly adding a one-carbon moiety can limit certain applications. Fluorine-18 (^{18}F) is widely used as a tracer radionuclide and benefits from advances in fluorine chemistry such that fluorine-18 can label drug molecules with surprising chemical reaction flexibility (Alauddin, 2012). However, the addition of a fluorine atom to a drug can alter the drug PK/PD characteristics if a fluorine-18 atom is a novel addition. Here, a battery of *in vitro* and *in vivo* studies is typically required to validate these new pharmacological properties. A key advantage to fluorine-18 is that it possesses a far greater half-life ($t_{½}$ = 110 min) than carbon-11 allowing for more sustained experimental evaluations and measures to be conducted. Since both carbon-11 and fluorine-18 radiolabeling transformations are efficient, both tracer types can be produced in high molar (specific) activity. This allows for remarkable tracer sensitivity measures while taking advantage of very short half-lives. Hence, studies in our laboratories have focused on both carbon-11 and fluorine-18 tracers.

3.5. Design and synthesis of organophosphorus PET tracers

The design and preparation of custom OP PET tracers was undertaken with the goal of examining: a) PK distributions, b) PD fates including the *in vivo* inactivation and labeling of AChE rich tissues, c) spatio-temporal imaging (Clarkson and Kupinski, 2009; Scarpelli et al., 2018) (*e.g.*, Fig. 4) and, d) conducting challenge studies in which displacement or blocking of the OP tracer from AChE-rich regions could be observed and quantified. Several design elements were considered in the development of OP PET tracers all requiring an understanding of the mechanism of action.

The approach focused on PET tracers of chemical agent 'surrogates' – OP compounds in which the leaving group of the chemical warfare agent (F, thiolester) has been exchanged for *p*-nitrophenyl (PNP) (Fig. 1). Replacement with the PNP group preserves the mechanism of inhibition (Fig. 2) (Chao et al., 2016; Chao et al., 2018; Meek et al., 2012) while reducing reactivity and volatility and conveniently adds a chromophore for analysis. The methyl–phosphonate bond and alkoxyester are retained as substituents in the surrogates.

As noted, OPs differ from most drugs converted into PET tracers because OPs bind their target (AChE) by formation of a largely irreversible, covalent bond. This process works synchronously with the ejection of a leaving group, so by design, the tracer atom cannot be part of the leaving group because once ejected it would not report on OP-modified AChE. Due to proximity and electronegativity considerations installing a fluorine-18 ([^{18}F]) radionuclide at the phosphonate methyl group as a P-CH_2F would alter the reactivity at phosphorus and alter the methylene (-CH_2-) acidity. Therefore, the alkoxy group was chosen for incorporation of the fluorine and eventual [^{18}F]OP surrogate tracer as it would afford OP-AChE adducts with the fluorine-18 attached to report on AChE (Fig. 2).

Although placement of a carbon-11 label at the phosphorus methyl group would afford a highly desirable OP tracer, the synthetic methods to create a carbon-phosphorus bond were considered incompatible with the short carbon-11 tracer lifetime. Given this obstacle, the alkoxy substituent was again chosen for placement of the [^{11}C]-radionucleide that in theory affords PET-labeled OP-AChE adducts with the tracer as shown for the fluoro-VX and fluoro–sarin surrogates (Fig. 2).

To prepare the fluorine-containing OP surrogates, [^{18}F]fluoroalcohols (Pan et al., 2013) or fluorotosylates were used (James et al., 2014; Neumann et al., 2017) in transesterification or alkylation processes. 2-Fluoroethanol and 1-fluoro-2-propanol were produced from fluoride ring opening of ethylene or propylene sulfite, respectively (Hayes et al., 2018). Reaction of each of the [^{18}F]fluoroalcohols with *O,O*-(*bis-p*-nitrophenyl) methylphosphonate in the presence of a hindered base (DBU) led to rapid transesterification (< 1 min) to yield the OP PET tracers bearing the [^{18}F]radionuclide at the alkoxy group (Scheme 2). This process was an improvement over our previously reported alkylation of the cesium salt of O-*p*-nitrophenyl methylphosphonic acid to prepare the [^{18}F]VX-surrogate.

For the preparation of the carbon-11 OP surrogates, the radionuclide was installed at the ethyl and isopropyl phosphorus ester positions. [^{11}C]-Ethyl and isopropyl iodides were both prepared from ^{11}[C]CO_2 and used to alkylate *O-p*-nitrophenyl methylphosphonic acid in a similar process to that used to prepare the F-VX surrogate from the tosylate except the iodides proved to be better reactants with the phosphonic acid salts (Scheme 3).

Overall, four OP radiotracers have been prepared to date including [^{11}C]VX- and [^{18}F]VX OP surrogates, and the [^{11}C]sarin- and [^{18}F]sarin OP surrogates. Two synthetic approaches were found to successfully install the tracer groups: (a) transesterification with *O,O-bis-p*-nitrophenoxy methyl phosphonate or, (b) alkylation of O-(p-nitrophenoxy) methyl phosphonic acid (Schemes 2 and 3). In all cases, excellent radiotracer purity was observed with high molar activity. With the radiolabeling methodology in hand to attach [^{11}C]ethoxy and [^{18}F]fluoroethoxy groups to phosphorus, the preparation of other PET tracers representing OP chemical warfare agents and insecticides are underway including [^{11}C]paraoxon and fluorine-18 analogs of other CWA surrogates.

It is important to realize that all of the radiotracer syntheses are under continual, iterative refinement and optimization. Although the radiotracer purity is at least 98% for both the reported processes, new methods come forward that increase molar activity and reduce impurities that not only lead to more reliable and reproducible experimentation but enable possible robotic automated conversion and routine tracer output.

3.6. Design and synthesis of oxime antidote PET tracers

From the prior section, it was shown that carbon-11 and fluorine-18 organophosphate PET radiotracers can be prepared. The availability of these tracers increase opportunities to evaluate OP toxicity in live subjects. As a complementary approach, oximes converted into radiotracers could identify differences in PK and PD measures for existing and new antidotes in the absence and presence of OP exposures.

For the oximes, only carbon-11 radiotracers were considered due to the potential difficulty of placing a fluorine atom on the N-alkyl pyridinium (methyl, *etc.*) or directly onto the pyridine ring as the resultant respective tracers would require investigations of changes to the

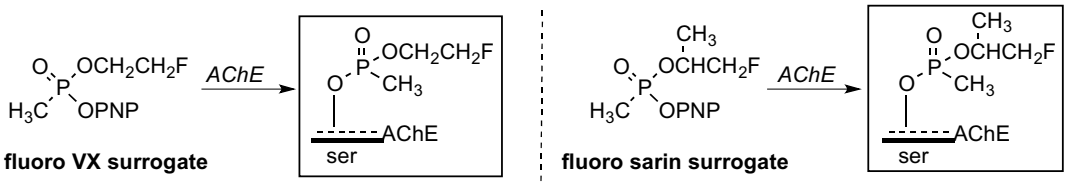

Fig. 2. Structures of the fluoro surrogates and the expected OP-AChE adducts formed. PNP = *p*-nitrophenyl.

pharmacokinetics relative to the parent oxime forms. Since N-alkylation radiolabeling reactions are well known (Antoni, 2015) the relative ease of installing a [^{11}C]-methyl directly onto the pyridine nitrogen to rapidly produce the tracer [^{11}C]2-PAM was considered viable. Therefore, the preparation of [^{11}C]2-PAM was accomplished by *N*-methylation of 2-pyridine-aldoxime using [^{11}C]CH_3-I, which is a well-known radiolabeling reagent and available in high molar activity from [^{11}C]CO. Still, the [^{11}C]2-PAM radiosynthesis required significant revision of non-radioactive methodology, because the reported non-radioactive synthesis used excess methyl iodide to induce the pyridyl-nitrogen alkylation and precipitate the product salt, which is not suitable for radiotracer work. Using polar, aprotic solvents (*e.g.*, DMF) at higher temperatures led to good conversion to [^{11}C]2-PAM (based on methyl iodide) using a 100-fold excess of pyridine-2-aldoxime. Further refinements in the radiosynthesis using acetonitrile in a sealed tube led to [^{11}C]2-PAM in good radiochemical yield, molar activity, and > 95% radiochemical purity in < 40 min (Scheme 4). Similarly, the preparations of other oxime radiotracers are feasible and currently underway.

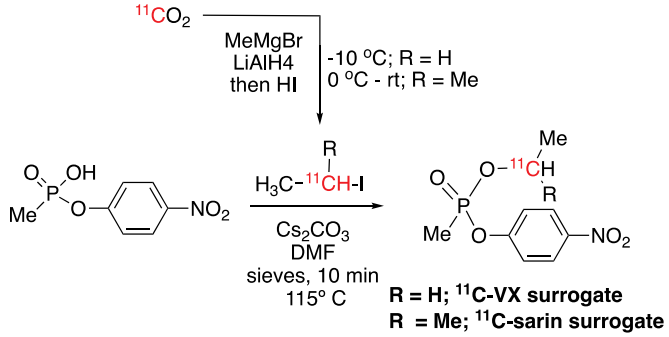

Scheme 3. Synthesis of carbon-11 organophosphate surrogates by reaction of ^{11}C-alkyl iodides with the cesium salt of O-*p*-nitrophenyl methylphosphonic acid.

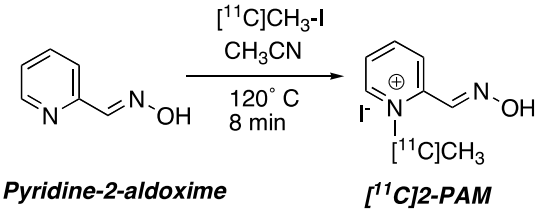

Scheme 4. Synthesis of ^{11}[C]-2-PAM.

4. ^{18}F-VX surrogate: O-(2-[^{18}F] fluoroethyl)-O-(*p*-nitrophenyl) methylphosphonate

The successful radiosynthesis of the [^{18}F]VX-surrogate generates the possibility for, tracer experiments in live animals. However, the usefulness of any tracer in which a fluorine atom has been added requires that the physico-chemical properties and, in this instance, the mechanism of inhibition be assessed before experiments are conducted in live subjects. If the fluorinated analog was unstable, and therefore unable to access CNS tissues at biologically-relevant levels or was a poor inhibitor of AChE, the effectiveness of the F-VX surrogate as tracer would be diminished. The demonstration that the F-VX surrogate has comparable stability to most OPs and is a potent anti-AChE inhibitor potency would permit a mechanistic precedent and advance complete *in vivo* evaluation of toxicokinetic properties and as a platform technology in rodents. In this section, the interactions of the unlabeled F-VX-surrogate with AChE are covered first followed by imaging studies with the [^{18}F]VX-surrogate.

4.1. AChE inhibition by the F-VX surrogate; role of fluorine

There are scant relevant examples of OPs bearing a P-O-CH_2CH_2X (X = halogen) group to compare anti-AChE potency with the F-VX surrogate, so neither chemical nor enzymatic reactivities could be readily predicted *a priori*. Nevertheless, addition of an electron-withdrawing fluorine to a phosphoester as in the F-VX surrogate might be expected to increase the reactivity at phosphorus with nucleophiles while suppressing reactions that occur under acid conditions.

Hydrolysis rates were determined for F-VX surrogate by measurement of displaced nitrophenolate anion (λ_{max} = 405 nm) (Chao et al., 2016). The stability of F-VX surrogate in phosphate buffered saline (PBS) at pH 7.4 afforded the pseudo first order rate constants (k_{obsd}) of 3.25×10^{-4} min^{-1} ($t_{½}$ = 35.6 h) at 25 °C and 8.70×10^{-4} min^{-1} ($t_{½}$ = 13.3 h) at 37 °C. Hydrolysis at 37 °C was slower than reported for $(CH_3)(CH_3CH_2O)P(O)OPNP$ with (k_{hyd}) = 2.42×10^{-3} min^{-1} ($t_{½}$ = 4.8 h) but this value was obtained at much higher pH 8.3 (Fukuto

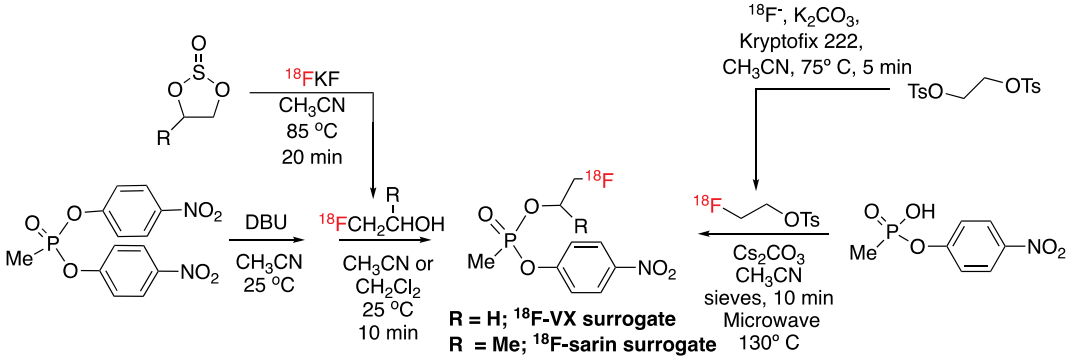

Scheme 2. Synthesis of fluorine-18 organophosphate surrogates by transesterification and alkylation.

and Metcalf, 1959). Overall, the hydrolysis rates indicate that F-VX surrogate is stable at pH 7.4 for the duration of PET experiments (*e.g.*, 1–6 h), but significant breakdown could occur over prolonged time. The rate constants for F-VX surrogate are comparable to triester OP compounds bearing a PNP group (*e.g.*, paraoxon) although the hydrolysis conditions differed (Cox and Ramsay, 1964). From the hydrolysis data, it was determined that the presence of the fluorine atom does not accelerate hydrolytic degradation, and was stable in solution for the *in vitro* enzyme assays, and similarly will be stable in PBS formulations used *in vivo* for the tracer [^{18}F]VX-surrogate.

The inhibition rate and mechanism of AChE inhibition by F-VX surrogate was studied against several cholinesterases (Chao et al., 2016; Kaleem Ahmed et al., 2013). The bimolecular inhibition rate constants (k_i) were determined for electric eel (EEAChE) $k_i = 4.2 \times 10^6\,M^{-1}\,min^{-1}$, recombinant human AChE $k_i = 1.1 \times 10^7\,M^{-1}\,min^{-1}$, recombinant human butyrylcholinesterase (HuBChE) $k_i = 1.95 \times 10^5\,M^{-1}\,min^{-1}$ and rat brain AChE $k_i = 6.1 \times 10^6\,M^{-1}\,min^{-1}$ indicating that the F-VX surrogate is a potent, *in vitro* inhibitor and 5-fold more potent than paraoxon against rat brain AChE.(Johnson and Wallace, 1987) Work by Chambers (Coban et al., 2016; Meek et al., 2012) also showed that (Me)(EtO)P(O)(OPNP) was a strong inhibitor ($k_i = 10^5\,M^{-1}\,min^{-1}$) of acetyl- and butyrylcholinesterases matching the mechanism of VX inhibition. The k_i values and likelihood of the PNP acting as leaving group strongly suggests that the mechanism of AChE inhibition proceeds *via* formation of the (2-fluoroethyl) methylphosphonate (Scheme 5) that would by analogy, afford ^{18}[F]-labeled enzyme from F-VX surrogate.

To validate the AChE-adduct formed from the F-VX surrogate, MALDI-TOF mass spectrometry analyses were conducted to identify the OP moiety attached to HuAChE or HuBChE. Following inhibition by the F-VX surrogate, the OP-ChE adducts were separated from surplus F-VX surrogate, digested with trypsin, and the peptide bearing the active site serine analyzed for mass changes. The predicted peptide masses for the monoisotopic ions would display the F-VX-surrogate modified peptide with a net mass increase by *m/z* 124. With both enzymes, the MeP(O)(OCH_2CH_2F)-O-serine peptides were identified (Table 1) with a mass increase of 124 indicating a mechanism in which the inhibition occurs with loss of the PNP leaving group. A time-dependent MALDI-TOF MS analyses of the VX- and F-VX modified peptides showed a steady reduction in the amount of adduct *versus* unmodified parent peptide suggesting initial formation of the adduct that undergoes reactivation over time (Chao et al., 2018).

4.2. The mechanism of AChE reactivation and aging following inhibition by the F-VX surrogate

To confirm that the *in vivo* studies with [^{18}F]VX-surrogate PET tracer represent stable modifications of cholinesterases, it was essential to ascertain the identity of the OP-AChE modification over the course of the tracer lifetime. As noted in the design, loss of the [^{18}F]labeled ester moiety to aging, for example, could afford pools of inhibited, yet unlabeled AChE that would alter or underestimate the dynamic measures. Therefore, the rate and extent of reactivation and aging of cholinesterases that were inhibited by the F-VX surrogate were conducted. Both spontaneous and oxime-mediated reactivation experiments were performed to parallel *in vivo* experiments representing baseline and countermeasure intervention. The aging rate is obtained from the non-reactivatable fraction of enzyme following the addition of oxime.

Spontaneous reactivation is a process whereby formation of the OP-cholinesterase adduct is reversed by scission of the phosphoserine bond without the aid of reactivating agents (Bajgar, 2004; Barthold and Schier, 2005; Fukuto, 1990b; Holstege et al., 1997; Kuca et al., 2010a; Taylor, 2018; Worek et al., 2008) and part or all of the catalytic activity is restored. Typically, OP-ChE adducts containing P-OMe or P-OEt groups undergo spontaneous reactivation in a few minutes to hours (Morita, 1995; Worek et al., 2008) whereas OP-ChE adducts with branched esters like P-OiPr or P-OCH(Me)C(Me)$_3$ reactivate slowly and/or undergo an alternate mechanism known as aging. Spontaneous reactivation also occurs at rates > 100-fold slower than oxime-mediated reactivation (*e.g.*, [2-PAM] = 1.0 μM) (Chao et al., 2016; Chao et al., 2018; Worek et al., 2008).

HuAChE or huBChE were treated with F-VX-surrogate (from 10 to 160 nM) to > 95% inhibition and the recovery of enzyme activity measured following dilution to halt further inhibition or possible re-inhibition. The spontaneous reactivation rate constants (k_r) for were $9.31 \times 10^{-5}\,min^{-1}$ ($t_{1/2}$ = 124 h; HuAChE) and $1.13 \times 10^{-4}\,min^{-1}$ ($t_{1/2}$ = 102 h; HuBChE), which data is in general agreement with k_r rates found for VX and the *p*-nitrophenoxy VX surrogates (Albuquerque et al., 2006; Coban et al., 2016; Kuca et al., 2010a; Sidell and Groff, 1974). The data implies that ChE-OP(O)(CH_3)(OCH_2CH_2F) adducts are stable and likely measurable *in vivo* as the corresponding [^{18}F]containing OP-AChE adduct over the lifetime of the tracer, although the lack of restoration of enzyme activity cannot be attributed solely to the ChE-OP(O)(CH_3)(OCH_2CH_2F) adduct.

Oxime-mediated reactivation of cholinesterases inhibited by the F-VX-surrogate was conducted with 2-PAM (10.0 μM; FDA-approved for OP exposure) (Chao et al., 2016; Chao et al., 2018). The reaction of the ChE-OP(O)(CH_3)(OCH_2CH_2F) inhibited adducts with 2-PAM was evaluated *in vitro* using the same inhibitor concentrations used for spontaneous reactivation. Following inhibition of huAChE or huBChE (0.16 nM) with F-VX surrogate at 30 min and then at 18 h, the enzymic activity was measured. HuAChE inhibited by F-VX surrogate underwent oxime-mediated reactivation of $2.40 \times 10^{-2}\,min^{-1}$ ($t_{½}$ = 0.48 h) and $2.47 \times 10^{-2}\,min^{-1}$ ($t_{½}$ = 0.47 h) at 30 min and 18 h, respectively. The rapid rate and extent of oxime-mediated reactivation suggests that aging does not occur to an appreciable extent. However, 12% aging was observed at 24 h in an *in vivo* study suggesting partial loss of the ethoxy group (Meek et al., 2012). Again, the fluorine atom present on the OP-ChE adduct may facilitate oxime-mediated reactivation and disfavor aging. Because the radiotracer would be introduced into the bloodstream, the reactivation rate of butyrylcholinesterase was also needed. HuBChE inhibited by F-VX surrogate underwent oxime-mediated reactivation at 30 min with rate constant $1.14 \times 10^{-2}\,min^{-1}$ ($t_{½}$ = 1.01 h) which was slower than at 18 h ($4.19 \times 10^{-2}\,min^{-1}$; $t_{½}$ = 0.27 h). However, both rates were found to be comparable to HuAChE and likely proceeding *via* a similar dephosphylation mechanism.

Overall, the *in vitro* reaction of F-VX surrogate with ChE's affords

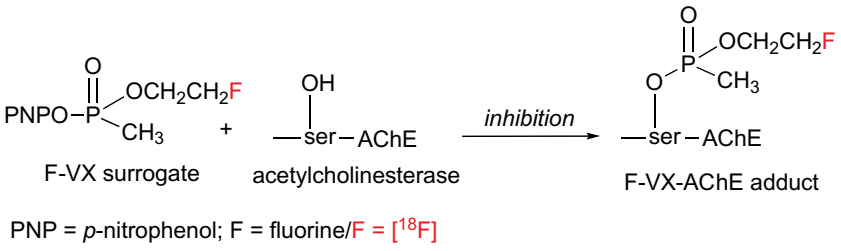

Scheme 5. Mechanism of AChE inhibition by the F-VX surrogate.

Table 1
Mass ions identified for unmodified and F-VX surrogate-modified tryptic peptides from HuAChE and HuBChE containing the active site serine.

Peptide or 'OP-adducted peptide'	Mass of peptide or OP-peptide adduct	OP-adduct identified as multiply-charged ion
HuAChE tryptic peptide A (unmodified)	4268.1445	1423.7148 (M^{3+})
peptide A - OP(O)(CH_3)(OCH_2CH_2F) (+124)	4392.1534	1465.0511 (M^{3+})
HuBChE tryptic peptide B (unmodified)	2928.5214	977.1738 (M^{3+})
peptide B - OP(O)(CH_3)(OCH_2CH_2F) (+ 124)	3052.5303	1018.5101 (M^{3+})

Peptide A = LALQWVQENVAAFGGDPTSVTLFGESAGAASVGMHLLSPPSR.
Peptide B = SVTLFGESAGAASVSLHLLSPGSHSLFTR.

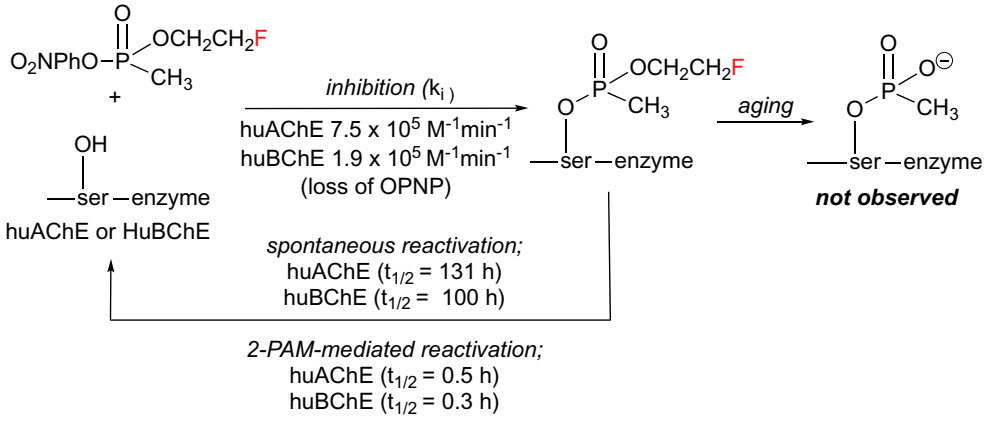

Scheme 6. Inhibition, reactivation and non-aging determinations and processes for HuAChE and HuBChE inhibited by F-VX surrogate.

beta-fluoroethoxy methylphosphonate adducts that undergo both spontaneous and oxime-mediated reactivation (Scheme 6). Spontaneous and oxime-mediated reactivation rates were comparable for both HuAChE and HuBChE and expectedly the oxime-mediated rates were 100- to 250-fold faster than spontaneous rates. Rate accelerations of 100-fold when using oximes for VX-inhibited cholinesterases have been reported (Forsberg and Puu, 1984; Kuca et al., 2010a; Kuca et al., 2010b). There was little difference in the oxime-mediated reactivation rates found at 30 min and 18 h, and in general, mammalian enzyme inactivated at > 95% of its' initial velocity fully recovered activity. This outcome is highly suggestive of an OP-ChE adduct that does not undergo aging. The process and rate values for inhibition, reactivation and aging are summarized in Scheme 6.

Although of low purity, electric eel AChE was used as a control enzyme due to its' fast substrate turnover and prolonged stability in solution, which allows for prolonged kinetic analyses. EEAChE undergoes spontaneous reactivation 100× faster than HuAChE when inhibited by F-VX surrogate and recovered almost 50% of the original activity within an hour (Chao et al., 2018). No evidence of aging was observed for F-VX surrogate inhibited EEAChE with > 99% of the original activity restored with 2-PAM. Rates derived with EEAChE are not applicable comparable to mammalian AChE but some point of comparison are worthy of note. For example, OP-AChE adducts formed from CWAs do not reactivate to the levels observed from F-VX surrogate due to a competing aging process. The nerve agent VX is an exception (Sidell and Groff, 1974) that yields an (EtO)(Me)P(O)-AChE adduct that is largely reactivatable but still undergoes some aging (Dorandeu et al., 2008; Kuca et al., 2010a; Meek et al., 2012; Shih et al., 2010a).

The difference in the AChE-VX and AChE-F-VX adducts is the *beta*-fluoro substituent that favors a nucleophilic process (water or an oxime). Cholinesterases inhibited by F-VX surrogate show no evidence of aging as evidenced by rapid reactivation and almost full restoration of activity following treatment with 2-PAM. The lack of aging for this adduct is likely due to the small ethyl ester combined with the electron-withdrawing fluorine that collectively suppress the cation-based mechanisms although an aging pathway cannot be ruled out *in vivo* as was reported for the VX surrogate compound (Meek et al., 2012). The *in vitro* findings support a mechanism of AChE inhibition by [^{18}F]VX-surrogate *in vivo* such that the [^{18}F]VX–AChE adducts will not undergo appreciable aging over the PET imaging experimental time course but could be reactivated if needed.

4.3. Imaging and biodistribution of ^{18}F-VX surrogate

The *in vitro* studies corroborated the protein targets, mechanism of interaction, identity and longevity of the adduct, and mode of action of F-VX surrogate. Collectively, the *in vitro* work established that the corresponding [^{18}F]VX-surrogate would exhibit robust and predictable performance measures as the dynamic imaging tracer, and provide deep insights as to the rate and extent of OP-modifications to AChE-rich tissues in the CNS. The *in vivo* fate of [^{18}F]VX-surrogate would be capable of correlating measurements as the OP-modified AChE adduct, which could address an unmet need in OP CNS tissue penetration and distribution mammals. Live brains have been previously evaluated using custom positron atom-labeled tracers that interact with AChE by mechanisms devoid of covalent bond formation (Kikuchi et al., 2007; Kikuchi et al., 2009; Kikuchi et al., 2010; Shinotoh et al., 2004; Volkow et al., 2001). For example, carbon-11 tracers fashioned as either AChE substrates or as reversible binding radioligands have been used for functional imaging (Kikuchi et al., 2007; Kikuchi et al., 2009; Kikuchi et al., 2010). However, the only known PET tracer based on an OP has been [^{11}C]sarin (Prenant and Crouzel, 1990), but to our knowledge reports of this tracer in animals have not been available in the literature.

In vivo CNS penetration and distribution determinations for [^{18}F]VX-surrogate was performed in parallel with magnetic resonance (MR) and micro-computed axial tomography (CT) scanning, where the MR-CT data defined anatomical locations which enabled definitions of cerebral regions of interest (ROIs) (Paxinos and Watson, 2007) (James et al., 2014). Radioactivity in the ROIs was then determined as standard uptake values (SUV) (Innis et al., 2007) for comparison across rat subjects and average CNS radioactivity signals measured as ROI over time.

A representative time-activity curve for cerebral SUV radioactivity

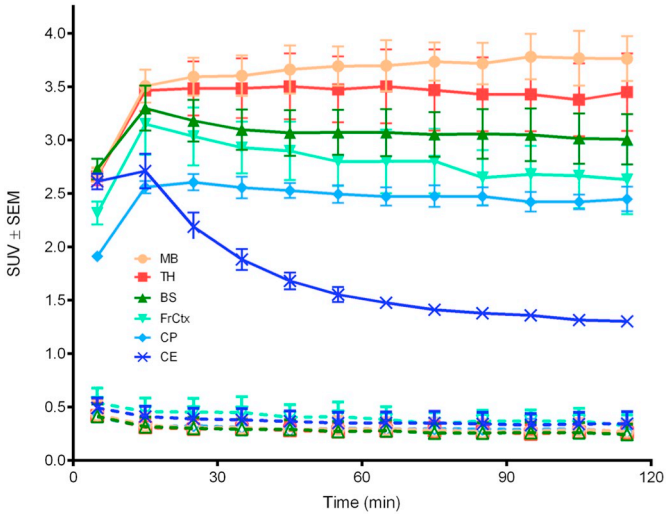

Fig. 3. SUV (normalized) radioactivity *vs.* time curves found in rat brain after i.v. injection of [^{18}F]VX-surrogate. Solid lines are tracer alone and broken lines are tracer and non-radioactive F-VX surrogate at 2.0 mg/kg (10 min prior). Legend: hind brain/brain stem (BS), caudate-putamen (CP), frontal cortex (FrCtx), mid-brain (MB), TH thalamus (TH), and cerebellum (CE). From James et al. *ACS Chem Neurosci.* 2014;5(7):519–24. Epub 2014/04/11. doi: https://doi.org/10.1021/cn500024c. PubMed PMID: 24716794; PMCID: 4102964. https://pubs.acs.org/doi/10.1021/cn500024c.

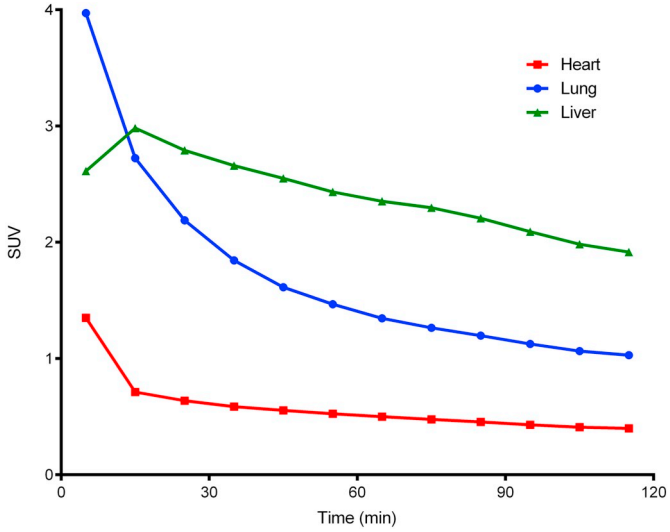

Fig. 5. Typical standard uptake value (SUV) *vs.* time curves for select peripheral rat tissues (heart, lung and liver; per legend) after administration of [^{18}F]VX-surrogate. From James et al. *ACS Chem Neurosci.* 2014;5(7):519–24. Epub 2014/04/11. doi: https://doi.org/10.1021/cn500024c. PubMed PMID: 24716794; PMCID: 4102964. https://pubs.acs.org/doi/10.1021/cn500024c.

profiles for the tracer alone from 0 to 120 min is demonstrated by solid lines (Fig. 3). The curves reveal rapid brain uptake of the tracer immediately after injection with ≥2.0 SUV (about 4% of injected dose) found in all ROIs between 0 and 30 min post tracer injection. Therefore, the [^{18}F]VX-surrogate readily penetrates brain after tail vein i.v. administration.

A sagittal brain image example as the summed radioactivity over 120 min with defined two-dimensional cerebral ROIs following tracer administration depicting the relative amount of tracer found in CNS (Fig. 4).

The Fig. 3 baseline (tracer only) time-radioactivity curves (solid lines) and the Fig. 4 image demonstrate differential radioactive signals in the ROIs after [^{18}F]VX-surrogate i.v. injection. At 60 min, high signals are found in mid-brain, thalamus and brain stem, with lower signals in the frontal cortex and caudate-putamen, and the lowest signal is found in the cerebellum. Brain ROIs except cerebellum equilibrate by 30 min and remain to 120 min. Interestingly, the decrease in cerebellum radioactivity more closely resembles peripheral tissues, especially lung (Fig. 5) that are characterized by an early maximum and then reduced radioactivity.

The observation that baseline (tracer only, Fig. 3) CNS time-radioactivity signals remain steady after 30 min suggests that the OP-inhibited AChE adduct ([^{18}F]CH_2CH_2O)(Me)P(O)-AChE has formed. The relative amounts of radioactivity per ROI in brain (Fig. 3) are consistent with relative regional cerebral rat AChE densities as determined by *ex vivo* histochemical measures (Biegon et al., 1986; Biegon and Wolff, 1986; Segal et al., 1988) and non-OP tracer AChE PET imaging profiling (Funaki et al., 2003; Planas et al., 1994; Ryu et al., 2005). As depicted in Fig. 4, it is important to note that no radioactivity was found in skull or bone suggesting that [^{18}F]fluoride ion was not liberated, otherwise [^{18}F]fluoride ion would have been rapidly assimilated into bone (Ametamey et al., 2008). The lack of free fluoride can be interpreted as the [^{18}F]β-fluoroethoxy of the F-VX surrogate and/or F-VX surrogate inhibited AChE remains intact during *in vivo* scanning.

To determine if the tracer interaction with AChE led to the adduct proposed *in vivo*, experiments using a competing, non-radioactive OP were needed. The ^{19}F-VX non-radioactive surrogate was selected for blocking experiments as it is the identical to the tracer and only slightly less potent than paraoxon as an AChE inhibitor (Chao et al., 2016; Chao et al., 2018). Pretreatment of rats with non-radioactive F-VX surrogate

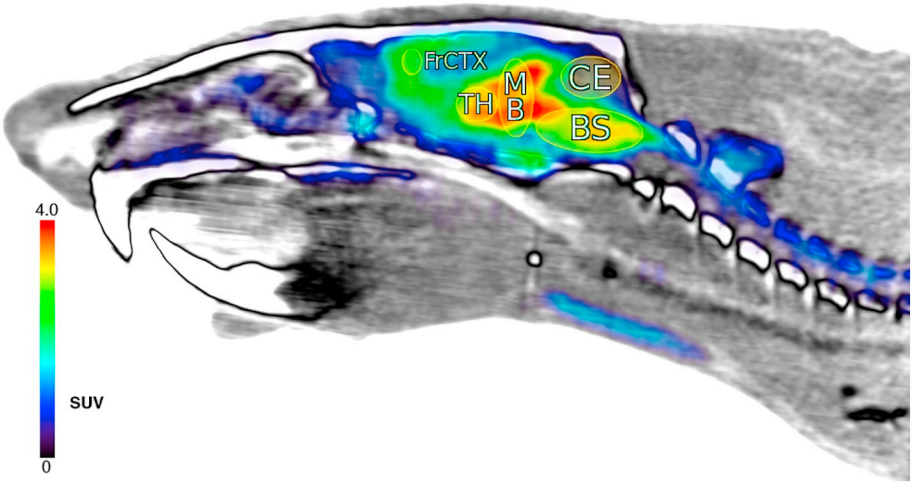

Fig. 4. Rat sagittal brain and partial spine view with PET radioactivity averaged over all timeframes (0–120 min) post [^{18}F]VX-surrogate i.v. injection. Image is displayed using NIH color table (0.0–4.0 SUV global thresholds); cerebral regions shown as ellipses and labeled per Fig. 3 definitions. From James et al. *ACS Chem Neurosci.* 2014;5(7):519–24. Epub 2014/04/11. doi: https://doi.org/10.1021/cn500024c. PubMed PMID: 24716794; PMCID: 4102964. https://pubs.acs.org/doi/10.1021/cn500024c.

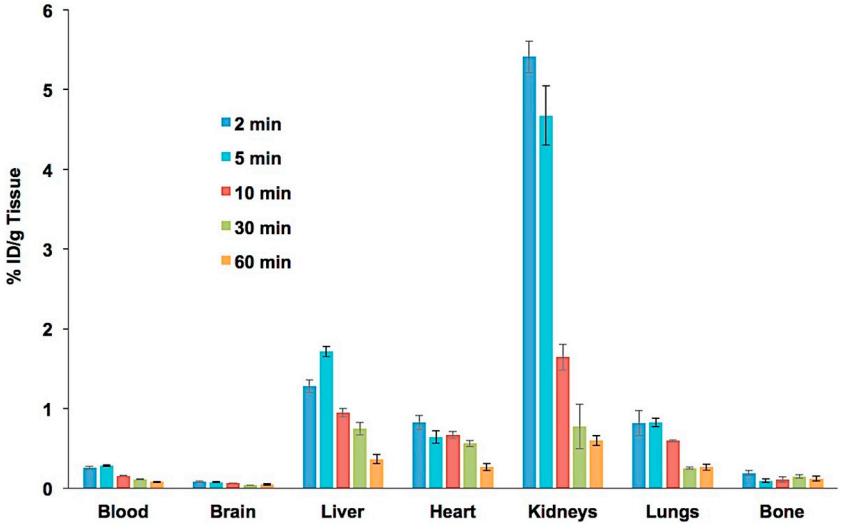

Fig. 6. Tracer alone as a baseline biodistribution (2–60 min) of decay-corrected radioactivity after [^{11}C]2-PAM tracer i.v. injection in naïve rats. From: A First-In-Class Antidote Tracer for Organophosphate Intoxication. From: Neumann et al. *ACS Chem Neurosci*. 2018. Epub 2018/08/04. doi: https://doi.org/10.1021/acschemneuro.8b00212. PubMed PMID: 30071719. https://pubs.acs.org/doi/10.1021/acschemneuro.8b00212.

ten minutes prior to injection of [^{18}F]VX-surrogate resulted in a significant reduction in radioactivity across all cerebral ROIs (Fig. 3, broken lines) relative to tracer alone (solid line curves). The differences between these two curve data sets suggest that pretreatment with non-radioactive ^{19}F-VX surrogate forms the OP-AChE adduct (FCH_2CH_2O)(Me)P(O)-AChE first, thereby blocking the isotopic [^{18}F]VX-surrogate from forming a radiolabeled AChE adduct. An explanation for the residual SUV ($\leq$ 0.5) observed in the challenge experiments remain less clear but it is possible that this low signal could be attributed, in part, to a radiolabeled fraction of the circulating blood or involves other tracer mechanistic processes in the tissues.

The [^{18}F]VX-surrogate PET tracer was designed to label and identify interactions at the target enzyme AChE in a living system while maintaining the mechanism of OP toxic action. The novel [^{18}F]VX-surrogate tracer quickly and effectively penetrates brain, and distributes to different regions of brain after 90 min that correlate to known AChE densities. At later time points, the CNS toxicokinetics remain constant which are consistent with the amount of fluorine-18-labeled-AChE covalent adduct formed. Although the fluorine-18-labeled OP is novel in that it reports on an OP-AChE adduct, further development of dynamic OP PET imaging technology is needed to identify and track *in vivo* mechanisms of action and the effect of countermeasures in relation to the radiolabeled adduct. For example, studies are underway to deploy the [^{18}F]VX-surrogate tracer to assess available AChE in CNS tissue after either exposure to other OP agents or treatment of OP exposure tissue with non-radioactive antidote oximes.

5. ^{11}C-2-PAM: [^{11}C] 2-Pyridine aldoximine methiodide

As discussed previously, oximes such as 2-PAM are used to counteract the action of toxic organophosphates by removing the phosphoryl moiety from the serine hydroxyl of AChE thus restoring its catalytic activity. The action of the oxime is effective so long as there is OP-inhibited AChE at the synapse, and therefore it is beneficial to maintain a therapeutic level of oxime over the first few hours of exposure to reverse inhibition and achieve clinical recovery. There are two key concerns to oxime therapeutics. First, oximes are largely ineffective when the OP-AChE inhibitor complex has undergone aging. Second, most oximes are quaternary amines and exist as charged cations that exhibit very low volume of distribution (< 1.0 L/kg) and short *in vivo* half -lives (~ 1 h) limiting blood brain barrier penetration; and thus, are with limited therapeutic action in the CNS. In terms of the limited action in brain, 2-PAM has been reported to enter rat brain in a dose-dependent manner in the absence of OP treatment (Sakurada et al., 2003) and that [^{14}C]2-PAM enters brain more readily following OP exposure (Firemark et al., 1964; Hobbiger and Vojvodic, 1967). Although 2-PAM enters brain at low levels, it is unclear how CNS levels might vary over time or as a function of OP exposure.

Still, it is well-established that an oxime be part of the overall standard of care to treat OP exposures along with a cholinergic blocker (*e.g.*, atropine) and anti-seizure medication (benzodiazepine). Thus, the role and efficacy of most clinically-approved oxime antidotes is to treat the peripheral toxicity where any amelioration of symptoms is considered beneficial. Citing these limitations, there has been a significant amount of development into new oxime and oxime-like therapeutics that can reactivate OP-aged cholinesterase or better access the CNS (brain penetrable). Before new antidotes can achieve clinical success, the PK/PD measures of new candidate therapeutics need to be evaluated in a dynamic, living system. The well-established, clinically-approved, antidote 2-PAM was an excellent candidate to convert into a first-in-class PET tracer to conduct initial measures and to create a novel platform technology and critically assess and compare with new countermeasures. A PET tracer based on the cation 2-PAM would permit, dynamic quantitative determinations in PNS and CNS tissues and a unique, *in vivo* perspective on therapeutics lacking a specific target in tissues not exposed to an OP. In addition to providing specific PK measures, a 2-PAM PET tracer could provide insights and measures in a dynamic system alone or as part of the standard of care, and/or in naïve *versus* OP-challenged animals. With [^{11}C]2-PAM tracer in hand, the evaluations included *ex vivo* biodistribution and *in vivo* dynamic PET imaging in rats (not exposed to OPs) for [^{11}C]2-PAM tracer alone and when tracer was co-injected with a therapeutic dose of non-radioactive 2-PAM. Under these conditions, the acquired data for [^{11}C] 2-PAM would enable correlations to previously established toxicology studies (Eddleston et al., 2008; Firemark et al., 1964; Jokanovic, 2012; Jokanovic and Prostran, 2009; Jokanovic and Stojiljkovic, 2006; Petrikovics et al., 2004; Sakurada et al., 2003; Shih et al., 2010a).

5.1. Biodistribution of [^{11}C]2-PAM

Biodistribution and PET imaging studies were performed on rats administered the tracer [^{11}C]2-PAM by tail vein i.v. injection under light isoflurane (1–2%). For the biodistribution study, baseline radioactivity profiles for blood, bone (femur) and select tissues were sampled up to 60 min after tracer injection (Fig. 6). The highest uptake was in kidney, lower amounts in liver, lung and heart, and lowest in blood, brain and bone. For all samples, time-dependent radioactivity uptake and washout profiles were observed over the 60 min experiment. Rapid uptake and washout are consistent with the lack of a high affinity 2-PAM target within the tissues and blood.

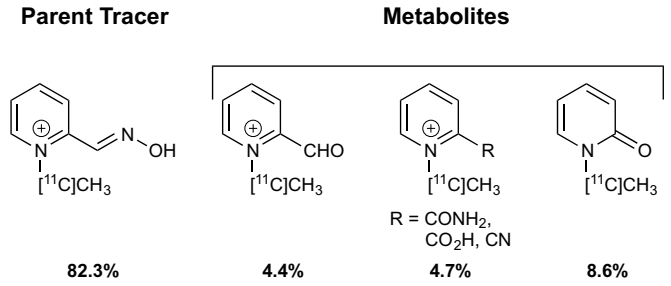

Fig. 7. Structure and distribution of metabolites present in the plasma free-fraction at 5 min after tracer injection.

Elevated radioactivity levels in kidney were anticipated for the highly water soluble 2-PAM and is associated with clearance (Gupta, 2015; Jovanovic, 1989). Limited uptake in brain is usually linked to the diminished ability of cationic [^{11}C]2-PAM to diffuse across the BBB (Firemark et al., 1964; Sakurada et al., 2003) and/or its'rapid export from the CNS. As only 10–15% of this radioactivity can be accounted for from the cerebral blood pool (Everett et al., 1956), the minimal brain radioactivity is thought to be mostly associated with tissue.

Since radioactivity levels in liver were highest at 5 min (Fig. 6), the amount of parent tracer relative to metabolites was determined at this time point. Tail artery blood sampling, processing and chromatographic profiling against chemical standards afforded the distribution of metabolites (Fig. 7) as follows. The serum showed 82% parent [^{11}C]2-PAM tracer and the remainder a mixture of the metabolites as follows: *N*-methyl-2- pyridinecarboxaldehyde (4.4%), a mixture of *N*-methyl-2-pyridinecarboxamide, *N*-methyl-2-pyridinecarboxylic acid, and *N*-methyl-2-pyridinecarbonitrile (4.7%), and *N*-methyl-2-pyridone (8.6%). The metabolite distribution is consistent with that reported previously (Enander et al., 1962; Firemark et al., 1964; Poziomek et al., 1958) in which the majority of recovered mass is 2-PAM with most metabolic changes occurring at the oxime functional group. Overall, the metabolite distribution provides some insight into the maximal 5 min liver biodistribution radioactivity profile.

5.2. Biodistribution of a therapeutic dosage of 2-PAM with [^{11}C]2PAM

Although there is significant value in understanding the PK/PD properties of OPs at tracer levels because even minute exposures can result in a potentially toxic event, oximes should be studied at or near the therapeutic dose to accurately represent the biodistribution profile that is applied following an OP exposure event. The study co-injected rats with a mixture of [^{11}C]2-PAM with 30 mg/kg (human therapeutic dose) of non-radioactive 2-PAM (Jokanovic, 2012; Jokanovic and Stojiljkovic, 2006; Sakurada et al., 2003), and the results (Fig. 8) were compared to baseline (tracer alone).

Statistical (one-way ANOVA) analyses revealed that there was no significant difference in tissue distributions at 5 min except liver (P = .0085) that may represent different effects on tracer metabolism in the absence *vs.* presence of 2-PAM. It is worthy to note that no significant difference in the uptake in brain radioactivity was observed when comparing tracer alone and tracer plus therapeutic 2-PAM dose. Overall, the biodistribution PK profiles from the [^{11}C]2-PAM tracer low mass doses closely resemble those observed with the therapeutic doses (Gupta, 2015; Jovanovic, 1989).

5.3. Imaging of [^{11}C]2-PAM with and without therapeutic levels of 2-PAM

PET imaging offers a powerful, complementary method to biodistribution in that it allows for dynamic evaluations of tissue radioactivity in live subjects. Somewhat experimentally constrained by the carbon-11 half-life of ~ 20 min, PET scan evaluations were conducted over 30 min, adjunct to CT and MR scan data to identify regional anatomical and tissue boundaries, and to conservatively define volumetric three-dimensional ROIs (Paxinos, 2015; Paxinos and Watson, 2007; Walker and Dominique, 1997). The radioactivity is determined as standardized uptake values (SUV) to provide consistency across rat subjects (Gambhir, 2004) *versus* time. The resultant time-activity curves (TACs) for tracer alone and tracer with non-radioactive 2-PAM data are shown in Figs. 9 and 10 along with a representative sagittal PET view of summed radioactivity (Fig. 11).

The baseline PET imaging plot (Fig. 9; Panel A) shows a similar profile to the *ex vivo* biodistribution data. When [^{11}C]2-PAM is co-injected with 30 mg/kg of 2-PAM (Fig. 9; Panel B) the biodistribution data was similar (Panel A *vs.* Panel B) with washout apparent by 25 min. The higher radioactivity levels in kidney and liver likely represents greater tissue reservoirs for the cationic 2-PAM and is associated with clearance and metabolism, respectively. The brain TACs (Fig. 10) for baseline and co-injection of 2-PAM are similar in that low levels of radioactive 2-PAM enter brain, and reach a steady concentration after 5 min. A slight decrease in brain levels when co-injected with unlabeled 2-PAM (Fig. 10) at equilibrium was expected due to overall dilution in circulating 2-PAM. Overall, the presence of a large excess of 2-PAM along with tracer does not influence the amount of radioactivity penetration into brain, which was anticipated without a specific target for 2-PAM to bind.

The PET imaging data shows that the carbon-11 half-life for [^{11}C]2-

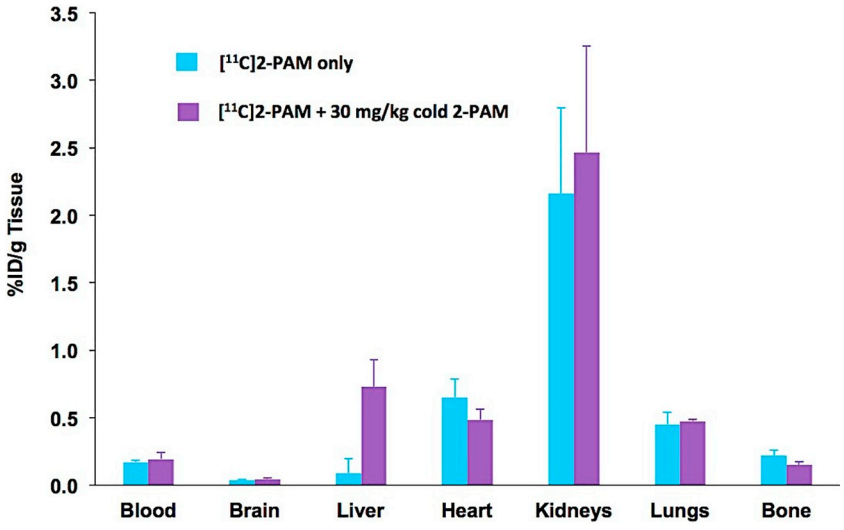

Fig. 8. Biodistribution comparison for [^{11}C]2-PAM (baseline, aqua) and [^{11}C]2-PAM co-injected with 30 mg/kg 2-PAM (purple) at 5 min. From: Neumann et al. *ACS Chem Neurosci*. 2018. Epub 2018/08/04. doi: https://doi.org/10.1021/acschemneuro.8b00212. PubMed PMID: 30071719. https://pubs.acs.org/doi/10.1021/acschemneuro.8b00212 (For interpretation of the references to color in this figure legend, the reader is referred to the web version of this article.)

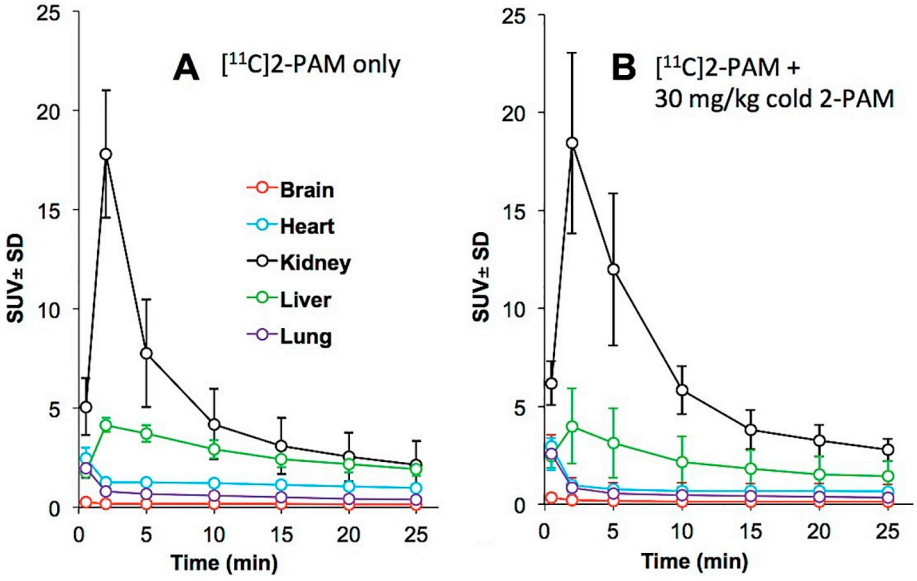

Fig. 9. PET imaging detected radioactivity *vs.* time (min) in rats. Panel A: [^{11}C]2-PAM tracer alone (baseline). Panel B: tracer co-injected with 30 mg/kg 2-PAM. From: Neumann et al. *ACS Chem Neurosci*. 2018. Epub 2018/08/04. doi: https://doi.org/10.1021/acschemneuro.8b00212. PubMed PMID: 30071719. https://pubs.acs.org/doi/10.1021/acschemneuro.8b00212.

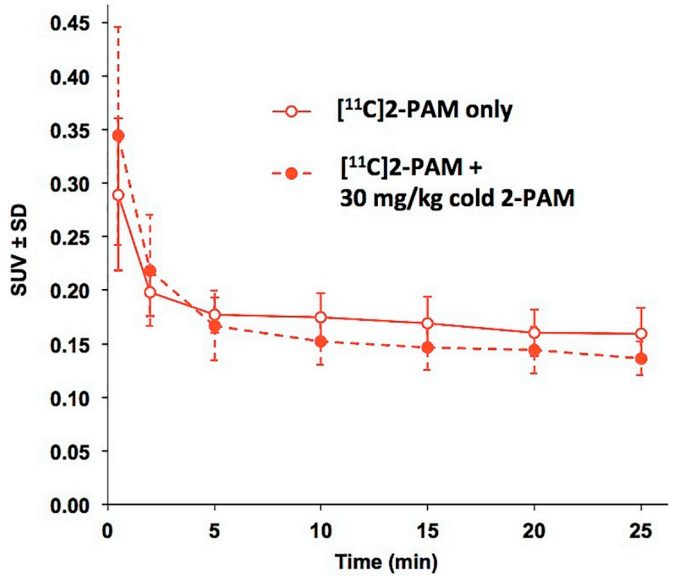

Fig. 10. Expanded view PET imaging time-activity curves in brain for [^{11}C]2-PAM tracer alone (baseline; open circles and solid line) and tracer co-injected with 30 mg/kg 2-PAM (solid points and dashed line). From: Neumann et al. *ACS Chem Neurosci*. 2018. Epub 2018/08/04. doi: https://doi.org/10.1021/acschemneuro.8b00212. PubMed PMID: 30071719. https://pubs.acs.org/doi/10.1021/acschemneuro.8b00212.

PAM was not an experimental impediment and suitable for quantitative PK measures and identifying washout time periods. The tracer can be prepared easily and administered safely and intravenously. The [^{11}C]2-PAM biodistribution data was consistent with that previously reported including the identification and realtive amounts of metabolites. Dynamic *in vivo* PET imaging using [^{11}C]2-PAM tracer alone or co-injected with 30 mg/kg 2-PAM revealed that CNS and peripheral tissue radioactivity distributions were very similar but not identical with notable tracer decreases in come tissues. With these fundamental profiles acquired with [^{11}C]2-PAM in rat and using similar experiments, there is now an opportunity to assess OP exposed rats with the tracer. Thus, similarities and differences found between naïve *vs.* OP exposed rats will report on key *in vivo* therapeutic PK/PD parameters for 2-PAM which will serve as foundational data for comparative use in relation to other radiolabeled oxime tracers.

6. Concluding remarks: potential of OP and oxime PET tracers to assess new and emerging countermeasures

The overarching rationale for this investigation has been to study, develop and eventually provide a number of technologies for an imaging-based platform that would enable the interrogation and selection of new and existing countermeasures to combat OP exposures. This goal required the preparation and study of a panel of PET tracers representing both reactive organophosphates and oxime antidotes that considers their tissue distributions, key mechanisms of actions and competing *in vivo* process. To date, we have reported the preparation of three different OP PET tracers bearing fluorine-18 or carbon-11

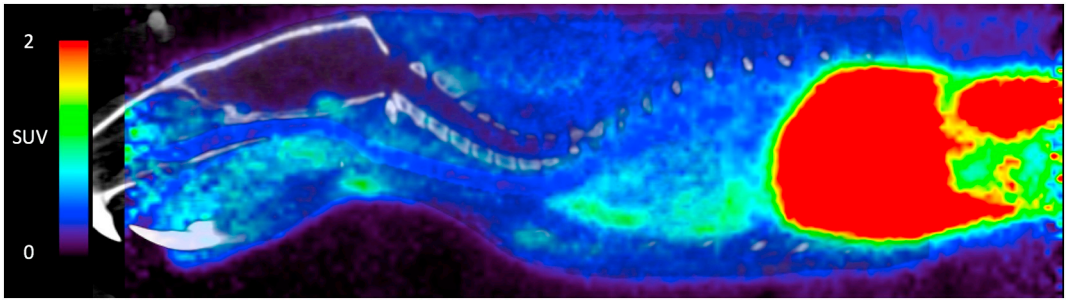

Fig. 11. PET-CT sagittal view of a 30 min summed radioactivity (SUV color bar) after injection of [^{11}C]2-PAM tracer alone (baseline). From: Neumann et al. *ACS Chem Neurosci*. 2018. Epub 2018/08/04. doi: https://doi.org/10.1021/acschemneuro.8b00212. PubMed PMID: 30071719. https://pubs.acs.org/doi/10.1021/acschemneuro.8b00212.

radionuclides and the antidote therapeutic carbon-11 2-PAM. Additional OP tracers representing chemical warfare agents and insecticides that react uniquely with AChE will be reported in due course.

Although one OP PET tracer would be sufficient to study the efficacy of a new countermeasure, the benefit to multiple OP PET tracer subtypes cannot be underestimated. For example, the [^{18}F]VX-surrogate yields an OP-AChE adduct that, due to the presence of the fluorine atom does not undergo appreciable aging and therefore is a stable, tracer-labeled enzyme adduct in the CNS. This is a highly useful, mechanistically-precise molecular probe to conduct displacement studies with oximes, especially those customized for improved brain penetration. OP PET tracers afford dynamic qualities at ultra-low doses that permit quantitative analyses in live tissues with rapid decomposition of the isotope. Because of the low detection levels, OP PET tracers can be used to conduct longitudinal and/or chronic exposure studies that are inherently problematic with toxic exposure doses or with other radioisotopes (*e.g.*, C-14, H-3, *etc.*). Due to their unique targeting and covalent action, OP PET tracers can also be used to assess residual or remaining AChE activity following exposure to other cholinesterase inhibitors. Such measures might be used to indirectly establish the exposure progress or conditional state of the brain, spine and peripheral nervous system tissues.

The prospect for additional oxime PET tracers is likely, yet less clear due to plausible synthetic limitations. However, [^{11}C]2-PAM itself is of potentially greater utility than originally thought. As mentioned, in naïve tissues 2-PAM is administered without a specific, high-binding target, and as such, is unique in PET imaging studies. Once an OP exposure occurs, 2-PAM is administered and serves largely as a peripheral reactivator. As 2-PAM penetrates brain poorly, the PK and imaging measures conducted provide an important CNS baseline by which other new countermeasures can be assessed both in peripheral and central tissues. The data regarding 2-PAM brain levels, although very low, establish a likely minimum by which other antidotes seeking to cross the BBB might be compared. With [^{11}C]2-PAM tissue measures now completed at tracer and tracer plus therapeutic level, any changes or additions to the standard of care can be measured relative to these baselines to determine if drug-drug interactions occur that might alter the PK of individual components or their biodistribution into key tissues.

Acknowledgments

The authors wish to thank their collaborators, H. VanBrocklin (UC San Francisco) and K. Zinn (Michigan State) as co-investigators on this project. Research reported in this publication was supported by the National Institute of Neurological Disorders and Stroke of the National Institutes of Health under Award Number U01NS092495. The content is solely the responsibility of the authors and does not necessarily represent the official views of the National Institutes of Health.

References

Ahn, K., et al., 2011. Mechanistic and pharmacological characterization of PF-04457845: a highly potent and selective fatty acid amide hydrolase inhibitor that reduces inflammatory and noninflammatory pain. J. Pharmacol. Exp. Ther. 338, 114–124.
Alauddin, M.M., 2012. Positron emission tomography (PET) imaging with (18)F-based radiotracers. Am. J. Nucl. Med. Mol. Imaging 2, 55–76.
Albuquerque, E.X., et al., 2006. Effective countermeasure against poisoning by organophosphorus insecticides and nerve agents. Proc. Natl. Acad. Sci. U. S. A. 103, 13220–13225.
Aldridge, W.N., Nemery, B., 1984. Toxicology of trialkylphosphorothioates with particular reference to lung toxicity. Fundam. Appl. Toxicol. 4, S215–S223.
Ames, R.G., et al., 1995. Chronic neurologic sequelae to cholinesterase inhibition among agricultural pesticide applicators. Arch. Environ. Health 50, 440–444.
Ametamey, S.M., et al., 2008. Molecular imaging with PET. Chem. Rev. 108, 1501–1516.
Antoni, G., 2015. Development of carbon-11 labelled PET tracers-radiochemical and technological challenges in a historic perspective. J. Label. Comp. Radiopharm. 58, 65–72.
Ashani, Y., et al., 1998. Combined effect of organophosphorus hydrolase and oxime on the reactivation rate of diethylphosphoryl-acetylcholinesterase conjugates. Biochem. Pharmacol. 55, 159–168.
Ashani, Y., et al., 2003. Inhibition of cholinesterases with cationic phosphonyl oximes highlights distinctive properties of the charged pyridine groups of quaternary oxime reactivators. Biochem. Pharmacol. 66, 191–202.
Bajgar, J., 2004. Organophosphates/nerve agent poisoning: mechanism of action, diagnosis, prophylaxis, and treatment. Adv. Clin. Chem. 38, 151–216.
Ballantyne, B., Marrs, T.C., 1992. Clinical and Experimental Toxicology of Organophosphates and Carbamates. Butterworth Heinemann, Oxford, Boston.
Barak, R., et al., 1997. Direct determination of the chemical composition of acetylcholinesterase phosphonylation products utilizing electrospray-ionization mass spectrometry. FEBS Lett. 407, 347–352.
Barthold, C.L., Schier, J.G., 2005. Organic phosphorus compounds–nerve agents. Crit. Care Clin. 21, 673–689 (v–vi).
Bedford, C.D., et al., 1986a. Nonquaternary cholinesterase reactivators. 3. 3(5)-substituted 1,2,4-oxadiazol-5(3)-aldoximes and 1,2,4-oxadiazole-5(3)-thiocarbohydroximates as reactivators of organophosphonate-inhibited eel and human acetylcholinesterase in vitro. J. Med. Chem. 29, 2174–2183.
Bedford, C.D., et al., 1986b. Nonquaternary cholinesterase reactivators. 4. Dialkylaminoalkyl thioesters of alpha-keto thiohydroximic acids as reactivators of ethyl methylphosphonyl- and 1,2,2-trimethylpropyl methylphosphonyl-acetylcholinesterase in vitro. J. Med. Chem. 29, 1689–1696.
Berkman, C.E., et al., 1993. Kinetics of the postinhibitory reactions of acetylcholinesterase poisoned by chiral isomalathion: a surprising nonreactivation induced by the RP stereoisomers. Chem. Res. Toxicol. 6, 28–32.
Berman, A., et al., 1995. Total alignment of calcite at acidic polydiacetylene films: cooperativity at the organic-inorganic interface. Science 269, 515–518.
Bharate, S.B., et al., 2010. Thionate versus Oxon: comparison of stability, uptake, and cell toxicity of ((14)CH(3)O)(2)-labeled methyl parathion and methyl paraoxon with SH-SY5Y cells. J. Agric. Food Chem. 58, 8460–8466.
Biegon, A., Wolff, M., 1986. Quantitative histochemistry of acetylcholinesterase in rat and human brain postmortem. J. Neurosci. Methods 16, 39–45.
Biegon, A., et al., 1986. Quantitative histochemistry of brain acetylcholinesterase and learning rate in the aged rat. Neurobiol. Aging 7, 215–217.
Black, R.M., et al., 1999. The interaction of sarin and soman with plasma proteins: the identification of a novel phosphonylation site. Arch. Toxicol. 73, 123–126.
Blomqvist, G., et al., 2001. Quantitative measurement of cerebral acetylcholinesterase using. J. Cereb. Blood Flow Metab. 21, 114–131.
Borsook, D., et al., 2013. Use of functional imaging across clinical phases in CNS drug development. Transl. Psychiatry 3, e282.
Carlson, K., Ehrich, M., 2004. Organophosphorus compound-induced delayed neurotoxicity in white leghorn hens assessed by Fluoro-jade. Int. J. Toxicol. 23, 259–266.
Casida, J.E., Quistad, G.B., 2004a. Organophosphate toxicology: safety aspects of non-acetylcholinesterase secondary targets. Chem. Res. Toxicol. 17, 983–998.
Casida, J.E., Quistad, G.B., 2004b. Organophosphate toxicology: safety aspects of non-acetylcholinesterase secondary targets. Chem. Res. Toxicol. 17, 983–998.
Casida, J.E., Quistad, G.B., 2005. Serine hydrolase targets of organophosphorus toxicants. Chem. Biol. Interact. 157–158, 277–283.
Chai, P.R., et al., 2017. Toxic chemical weapons of assassination and warfare: nerve agents VX and sarin. Toxicol. Commun. 1, 21–23.
Chambers, J.E., et al., 2013. Testing of novel brain-penetrating oxime reactivators of acetylcholinesterase inhibited by nerve agent surrogates. Chem. Biol. Interact. 203, 135–138.
Chambers, J.E., et al., 2016a. Efficacy of novel phenoxyalkyl pyridinium oximes as brain-penetrating reactivators of cholinesterase inhibited by surrogates of sarin and VX. Chem. Biol. Interact. 259, 154–159.
Chambers, J.E., et al., 2016b. Novel substituted phenoxyalkyl pyridinium oximes enhance survival and attenuate seizure-like behavior of rats receiving lethal levels of nerve agent surrogates. Toxicology 339, 51–57.
Chambers, J.E., et al., 2016c. Novel brain-penetrating oximes for reactivation of cholinesterase inhibited by sarin and VX surrogates. Ann. N. Y. Acad. Sci. 1374, 52–58.
Chao, C.K., et al., 2016. Novel organophosphate ligand O-(2-Fluoroethyl)-O-(p-Nitrophenyl)Methylphosphonate: synthesis, hydrolytic stability and analysis of the inhibition and reactivation of cholinesterases. Chem. Res. Toxicol. 29, 1810–1817.
Chao, C.K., et al., 2018. The inhibition, reactivation and mechanism of VX-, sarin-, fluoro-VX and fluoro-sarin surrogates following their interaction with HuAChE and HuBuChE. Chem. Biol. Interact. 291, 220–227.
Clarkson, E., Kupinski, M.A., 2009. Global compartmental pharmacokinetic models for spatiotemporal SPECT and PET imaging. SIAM J. Imag. Sci. 2, 203–225.
Coban, A., et al., 2016. Comparison of inhibition kinetics of several organophosphates, including some nerve agent surrogates, using human erythrocyte and rat and mouse brain acetylcholinesterase. Toxicol. Lett. 248, 39–45.
Collombet, J.M., 2011. Nerve agent intoxication: recent neuropathophysiological findings and subsequent impact on medical management prospects. Toxicol. Appl. Pharmacol. 255, 229–241.
Cox, J.R., Ramsay, O.B., 1964. Mechanisms of nucleophilic substitution in phosphate esters. Chem. Rev. 64, 317–352.
Cunningham, V.J., Lammertsma, A.A., 1994. Radioligand studies in brain: kinetic analysis of PET data. Med. Chem. Res. 5, 79–96.
Darvesh, S., 2013. Butyrylcholinesterase radioligands to image Alzheimer's disease brain. Chem. Biol. Interact. 203, 354–357.
de Koning, M.C., et al., 2011. Peripheral site ligand conjugation to a non-quaternary oxime enhances reactivation of nerve agent-inhibited human acetylcholinesterase. Toxicol. Lett. 206, 54–59.
Dementi, B., 1994. Ocular effects of organophosphates: a historical perspective of Saku disease. J. Appl. Toxicol. 14, 119–129.
Deshpande, L.S., et al., 2016. Pharmacological blockade of the calcium plateau provides

neuroprotection following organophosphate paraoxon induced status epilepticus in rats. Neurotoxicol. Teratol. 56, 81–86.
Ding, Y.S., Fowler, J., 2005. New-generation radiotracers for nAChR and NET. Nucl. Med. Biol. 32, 707–718.
Ding, Y.S., et al., 2005. Comparative evaluation of positron emission tomography radiotracers for imaging the norepinephrine transporter: (S,S) and (R,R) enantiomers of reboxetine analogs ([11C]methylreboxetine, 3-Cl-[11C]methylreboxetine and [18F]fluororeboxetine), (R)-[11C]nisoxetine, [11C]oxaprotiline and [11C]lortalamine. J. Neurochem. 94, 337–351.
Ding, Y.S., et al., 2006. PET imaging of norepinephrine transporters. Curr. Pharm. Des. 12, 3831–3845.
Dorandeu, F., et al., 2008. An unexpected plasma cholinesterase activity rebound after challenge with a high dose of the nerve agent VX. Toxicology 248, 151–157.
Dyer, S.M., et al., 2001. Peripheral cholinesterase inhibition by occupational chlorpyrifos exposure in Australian termiticide applicators. Toxicology 169, 177–185.
Eckelman, W.C., Mathis, C.A., 2006a. Molecular targets. Nucl. Med. Biol. 33, 1.
Eckelman, W.C., Mathis, C.A., 2006b. Targeting proteins in vivo: in vitro guidelines. Nucl. Med. Biol. 33, 161–164.
Eckelman, W.C., et al., 2006. Discussion of targeting proteins in vivo: in vitro guidelines. Nucl. Med. Biol. 33, 449–451.
Eddleston, M., et al., 2008. Management of acute organophosphorus pesticide poisoning. Lancet 371, 597–607.
Elhanany, E., et al., 2001. Resolving pathways of interaction of covalent inhibitors with the active site of acetylcholinesterases: MALDI-TOF/MS analysis of various nerve agent phosphyl adducts. Chem. Res. Toxicol. 14, 912–918.
Enander, I., et al., 1962. Metabolic studies on N-methylpyridinium-2-aldoxime. III. Experiments with the 14C-labelled compound. Biochem. Pharmacol. 11, 377–382.
Everett, N.B., et al., 1956. Distribution of blood (Fe 59) and plasma (I 131) volumes of rats determined by liquid nitrogen freezing. Circ. Res. 4, 419–424.
Firemark, H., et al., 1964. The penetration of 2-Pam-C14 into brain and the effect of cholinesterase inhibitors on its transport. J. Pharmacol. Exp. Ther. 145, 252–265.
Forsberg, A., Puu, G., 1984. Kinetics for the inhibition of acetylcholinesterase from the electric eel by some organophosphates and carbamates. Eur. J. Biochem. 140, 153–156.
Frangioni, J.V., 2006. Translating in vivo diagnostics into clinical reality. Nat. Biotechnol. 24, 909–913.
Frankle, W.G., et al., 2004. Comparative evaluation of serotonin transporter radioligands 11C-DASB and 11C-McN 5652 in healthy humans. J. Nucl. Med. 45, 682–694.
Fukuto, T.R., 1990a. Mechanism of action of organophosphorus and carbamate insecticides. Environ. Health Perspect. 87, 245–254.
Fukuto, T.R., 1990b. Mechanism of action of organophosphorus and carbamate insecticides. Environ. Health Perspect. 87, 245–254.
Fukuto, T.R., Metcalf, R.L., 1959. The effect of structure on the reactivity of alkylphosphonate esters1,2. J. Am. Chem. Soc. 81, 372–377.
Funaki, Y., et al., 2003. Evaluation of the binding characteristics of [5-(11)C-methoxy] donepezil in the rat brain for in vivo visualization of acetylcholinesterase. J. Pharmacol. Sci. 91, 105–112.
Gallo, M.A., Lawryk, N.J., 1991. Organic Phosphorus Pesticides. Academic Press, San Diego.
Gambhir, S.S., 2004. Quantitative assay development for PET. In: Phelps, M.E. (Ed.), Molecular Imaging and its Biological Applications. Springer, New York, NY, pp. 130–132.
Gearhart, J.M., et al., 1994. Physiologically based pharmacokinetic model for the inhibition of acetylcholinesterase by organophosphate esters. Environ. Health Perspect. 102 (Suppl. 11), 51–60.
George, K.M., et al., 2003. Differentiation between acetylcholinesterase and the organophosphate-inhibited form using antibodies and the correlation of antibody recognition with reactivation mechanism and rate. J. Biol. Chem. 278, 45512–45518.
Goncharov, N.V., et al., 2017. Serum albumin binding and esterase activity: mechanistic interactions with organophosphates. Molecules 22, 1201.
Grigoryan, H., et al., 2008. Mass spectrometry identifies covalent binding of soman, sarin, chlorpyrifos oxon, diisopropyl fluorophosphate, and FP-biotin to tyrosines on tubulin: a potential mechanism of long term toxicity by organophosphorus agents. Chem. Biol. Interact. 175, 180–186.
Grigoryan, H., et al., 2009. Mass spectrometry identifies multiple organophosphorylated sites on tubulin. Toxicol. Appl. Pharmacol. 240, 149–158.
Gupta, R.C., 2015. Handbook of Toxicology of Chemical Warfare Agents. Elsevier/AP, Academic Press is an imprint of Elsevier, Amsterdam; Boston.
Hayes, T.R., et al., 2018. Radiosynthesis of O-(1-[18F]fluoropropan-2-yl)-O-(4-nitrophenyl)methylphosphonate: a novel PET tracer surrogate of sarin. J. Label. Compd. Radiopharm. 61, 1089–1094.
Heiss, W.D., Herholz, K., 2006. Brain receptor imaging. J. Nucl. Med. 47, 302–312.
Hesse, S., et al., 2004. Advances in in vivo imaging of serotonergic neurons in neuropsychiatric disorders. Neurosci. Biobehav. Rev. 28, 547–563.
Hiraoka, K., et al., 2009. Quantitative analysis of donepezil binding to acetylcholinesterase using positron emission tomography and [5-(11)C-methoxy]donepezil. Neuroimage 46, 616–623.
Hobbiger, F., Vojvodic, V., 1967. The reactivation by pyridium aldoximes of phosphorylated acetylcholinesterase in the central nervous system. Biochem. Pharmacol. 16, 455–462.
Holstege, C.P., et al., 1997. Chemical warfare. Nerve agent poisoning. Crit. Care Clin. 13, 923–942.
Imamura, T., Gandy, J., 1988. Pulmonary toxicity of phosphorothioate impurities found in organophosphate insecticides. Pharmacol. Ther. 38, 419–427.
Imamura, T., Hasegawa, L., 1984. Role of metabolic activation, covalent binding, and glutathione depletion in pulmonary toxicity produced by an impurity of malathion. Toxicol. Appl. Pharmacol. 72, 476–483.
Innis, R.B., et al., 2007. Consensus nomenclature for in vivo imaging of reversibly binding radioligands. J. Cereb. Blood Flow Metab. 27, 1533–1539.
James, S.L., et al., 2014. A novel fluorine-18 beta-fluoroethoxy organophosphate positron emission tomography imaging tracer targeted to central nervous system acetylcholinesterase. ACS Chem. Neurosci. 5, 519–524.
John, H., et al., 2018. Fatal sarin poisoning in Syria 2013: forensic verification within an international laboratory network. Forensic Toxicol. 36, 61–71.
Johnson, J.A., Wallace, K.B., 1987. Species-related differences in the inhibition of brain acetylcholinesterase by paraoxon and malaoxon. Toxicol. Appl. Pharmacol. 88, 234–241.
Jokanovic, M., 2012. Structure-activity relationship and efficacy of pyridinium oximes in the treatment of poisoning with organophosphorus compounds: a review of recent data. Curr. Top. Med. Chem. 12, 1775–1789.
Jokanovic, M., Prostran, M., 2009. Pyridinium oximes as cholinesterase reactivators. Structure-activity relationship and efficacy in the treatment of poisoning with organophosphorus compounds. Curr. Med. Chem. 16, 2177–2188.
Jokanovic, M., Stojiljkovic, M.P., 2006. Current understanding of the application of pyridinium oximes as cholinesterase reactivators in treatment of organophosphate poisoning. Eur. J. Pharmacol. 553, 10–17.
Jovanovic, D., 1989. Pharmacokinetics of pralidoxime chloride. A comparative study in healthy volunteers and in organophosphorus poisoning. Arch. Toxicol. 63, 416–418.
Kaleem Ahmed, S., et al., 2013. Synthesis and anti-acetylcholinesterase properties of novel beta- and gamma-substituted alkoxy organophosphonates. Bioorg. Med. Chem. Lett. 23, 2048–2051.
Kamijima, M., Casida, J.E., 1999. Localization of [3H]octylphosphonyl-labeled neuropathy target esterase by chicken nervous tissue autoradiography. Neurosci. Lett. 273, 101–104.
Kikuchi, T., et al., 2007. Cerebral acetylcholinesterase imaging: development of the radioprobes. Curr. Top. Med. Chem. 7, 1790–1799.
Kikuchi, T., et al., 2009. In vivo evaluation of N-[(18)F]fluoroethylpiperidin-4ylmethyl acetate in rats compared with MP4A as a probe for measuring cerebral acetylcholinesterase activity. Synapse 64, 209–215.
Kikuchi, T., et al., 2010. In vivo evaluation of N-[18F]fluoroethylpiperidin-4ylmethyl acetate in rats compared with MP4A as a probe for measuring cerebral acetylcholinesterase activity. Synapse 64, 209–215.
Koeppe, R.A., et al., 1999. Kinetic modeling of N-[11C]methylpiperidin-4-yl propionate: alternatives for analysis of an irreversible positron emission tomography trace for measurement of acetylcholinesterase activity in human brain. J. Cereb. Blood Flow Metab. 19, 1150–1163.
Kuca, K., et al., 2010a. Reactivation of VX-inhibited AChE by novel oximes having two oxygen atoms in the linker. Environ. Toxicol. Pharmacol. 30, 85–87.
Kuca, K., et al., 2010b. Pralidoxime—the gold standard of acetylcholinesterase reactivators—reactivation in vitro efficacy. Bratisl. Lek. Listy 111, 502–504.
Laakso, A., Hietala, J., 2000. PET studies of brain monoamine transporters. Curr. Pharm. Des. 6, 1611–1623.
Langenberg, J.P., et al., 1988. Spontaneous and oxime-induced reactivation of acetylcholinesterase inhibited by phosphoramidates. Arch. Toxicol. 62, 305–310.
Lanks, K.W., Seleznick, M.J., 1981. Spontaneously reactivation of acetylcholinesterase inhibited by diisopropylfluorophosphate. Biochim. Biophys. Acta 660, 91–95.
Laruelle, M., et al., 2002. Positron emission tomography: imaging and quantification of neurotransporter availability. Methods 27, 287–299.
Laruelle, M., et al., 2003. Relationships between radiotracer properties and image quality in molecular imaging of the brain with positron emission tomography. Mol. Imaging Biol. 5, 363–375.
Leader, H., et al., 1999. Characterization of O,O-diethylphosphoryl oximes as inhibitors of cholinesterases and substrates of phosphotriesterases. Biochem. Pharmacol. 58, 503–515.
Lenz, D.L., et al., 1983. In Vivo Distribution of 14C-Soman in Rat. Am Soc Pharmacol & Exp Therap Meeting. Philadelphia, PA.
Lieske, C.N., Clark, J.H., Meyer, H.G., Lowe, J.R., 1980. Spontaneous and induced reactivation of Eel acetylcholinesterase inhibited by three Organophosphinates. Pestic. Biochem. Physiol. 13, 205–212.
Little, P.J., et al., 1986. Tissue disposition of [3H]sarin and its metabolites in mice. Toxicol. Appl. Pharmacol. 83, 412–419.
Logan, J., 2000. Graphical analysis of PET data applied to reversible and irreversible tracers. Nucl. Med. Biol. 27, 661–670.
Logan, J., et al., 1990. Graphical analysis of reversible radioligand binding from time-activity measurements applied to [N-11C-methyl]-(−)-cocaine PET studies in human subjects. J. Cereb. Blood Flow Metab. 10, 740–747.
Logan, J., et al., 2005. Modeling and analysis of PET studies with norepinephrine transporter ligands: the search for a reference region. Nucl. Med. Biol. 32, 531–542.
Lotti, M., Moretto, A., 1999. Promotion of organophosphate induced delayed polyneuropathy by certain esterase inhibitors. Chem. Biol. Interact. 119-120, 519–524.
Martin, B.R., 1985. Biodisposition of [3H]diisopropylfluorophosphate in mice. Toxicol. Appl. Pharmacol. 77, 275–284.
McCarren, H.S., et al., 2018. Dexmedetomidine stops benzodiazepine-refractory nerve agent-induced status epilepticus. Epilepsy Res. 141, 1–12.
Meek, E.C., et al., 2012. Synthesis and in vitro and in vivo inhibition potencies of highly relevant nerve agent surrogates. Toxicol. Sci. 126, 525–533.
Meinert, R., et al., 2000. Leukemia and non-Hodgkin's lymphoma in childhood and exposure to pesticides: results of a register-based case-control study in Germany. Am. J. Epidemiol. 151, 639–646 (discussion 647-50).
Michel, H.O., et al., 1967. Ageing and dealkylation of Soman (pinacolylmethylphosphonofluoridate)-inactivated eel cholinesterase. Arch. Biochem. Biophys. 121, 29–34.

Millard, C.B., et al., 1999. Crystal structures of aged phosphonylated acetylcholinesterase: nerve agent reaction products at the atomic level. Biochemistry 38, 7032–7039.
Moretto, A., Lotti, M., 1998. Poisoning by organophosphorus insecticides and sensory neuropathy. J. Neurol. Neurosurg. Psychiatry 64, 463–468.
Morita, H., 1995. Neurotoxicity of nerve agents. Brain Nerve 47, 1129–1134.
Musachio, J.L., et al., 2002. Radiosynthesis and mouse brain distribution studies of [11C] CP-126,998: a PET ligand for in vivo study of acetylcholinesterase. Nucl. Med. Biol. 29, 547–552.
Neumann, K.D., et al., 2017. An improved radiosynthesis of O-(2-[(18) F]fluoroethyl)-O-(p-nitrophenyl)methylphosphonate: a first-in-class cholinesterase PET tracer. J. Label. Comp. Radiopharm. 60, 337–342.
Niquet, J., et al., 2017a. Simultaneous triple therapy for the treatment of status epilepticus. Neurobiol. Dis. 104, 41–49.
Niquet, J., et al., 2017b. Treatment of experimental status epilepticus with synergistic drug combinations. Epilepsia 58, e49–e53.
Ohbu, S., et al., 1997. Sarin poisoning on Tokyo subway. South. Med. J. 90, 587–593.
Okumura, T., et al., 1996. Report on 640 victims of the Tokyo subway sarin attack. Ann. Emerg. Med. 28, 129–135.
Okumura, T., et al., 2005a. Acute and chronic effects of sarin exposure from the Tokyo subway incident. Environ. Toxicol. Pharmacol. 19, 447–450.
Okumura, T., et al., 2005b. The Tokyo subway sarin attack–lessons learned. Toxicol. Appl. Pharmacol. 207, 471–476.
Okuno, S., et al., 2008. Blood-brain barrier penetration of novel pyridinealdoxime methiodide (PAM)-type oximes examined by brain microdialysis with LC-MS/MS. Toxicol. Appl. Pharmacol. 227, 8–15.
Ordentlich, A., et al., 1999. Exploring the active center of human acetylcholinesterase with stereomers of an organophosphorus inhibitor with two chiral centers. Biochemistry 38, 3055–3066.
Pan, J., et al., 2013. f-[18F]fluoroethanol and 3-[18F]fluoropropanol: facile preparation, biodistribution in mice, and their application as nucleophiles in the synthesis of [18F] fluoroalkyl aryl ester and ether PET tracers. Nucl. Med. Biol. 40, 850–857.
Pappata, S., et al., 1996. In vivo imaging of human cerebral acetylcholinesterase. J. Neurochem. 67, 876–879.
Paxinos, G., 2015. Preface. The Rat Nervous System, Fourth edition. Academic Press, San Diego (pp. xi).
Paxinos, G., Watson, C., 2007. The Rat Brain in Stereotaxic Coordinates. Academic Press/Elsevier, Amsterdam; Boston.
Peeples, E.S., et al., 2005. Albumin, a new biomarker of organophosphorus toxicant exposure, identified by mass spectrometry. Toxicol. Sci. 83, 303–312.
Petrikovics, I., et al., 2004. Comparing therapeutic and prophylactic protection against the lethal effect of paraoxon. Toxicol. Sci. 77, 258–262.
Planas, A.M., et al., 1994. Rat brain acetylcholinesterase visualized with [11C]physostigmine. Neuroimage 1, 173–180.
Poziomek, E.J., et al., 1958. Pyridinium Aldoximes1. J. Org. Chem. 23, 714–717.
Prenant, C., Crouzel, C., 1990. Synthesis of [11C]-sarin. J. Label. Compd. Radiopharm. 28, 645–651.
Radic, Z., et al., 2012. Refinement of structural leads for centrally acting oxime reactivators of phosphylated cholinesterases. J. Biol. Chem. 287, 11798–11809.
Richardson, R.J., et al., 2013. Neuropathy target esterase (NTE): overview and future. Chem. Biol. Interact. 203, 238–244.
Ryu, S.M., et al., 1991. Comparative anticholinesterase potency of chiral isoparathion methyl. Chem. Res. Toxicol. 4, 517–520.
Ryu, E.K., et al., 2005. Synthesis and evaluation of 2-[18F]fluoro-CP-118,954 for the in vivo mapping of acetylcholinesterase. Nucl. Med. Biol. 32, 185–191.
Sakurada, K., et al., 2003. Pralidoxime iodide (2-PAM) penetrates across the blood-brain barrier. Neurochem. Res. 28, 1401–1407.
Scarpelli, M., et al., 2018. Dynamic 18F-FLT PET imaging of spatiotemporal changes in tumor cell proliferation and vasculature reveals the mechanistic actions of anti-angiogenic therapy. Phys. Med. Biol. 63, 155008.
Schuz, J., et al., 2000. Risk of childhood leukemia and parental self-reported occupational exposure to chemicals, dusts, and fumes: results from pooled analyses of German population-based case-control studies. Cancer Epidemiol. Biomark. Prev. 9, 835–838.
Segal, M., et al., 1988. A correlation between regional acetylcholinesterase activity in rat brain and performance in a spatial task. Behav. Brain Res. 30, 215–219.
Shapira, S., et al., 1990. Effects of CBDP and MEPQ on the toxicity and distribution of [3H]-soman in mice. Arch. Toxicol. 64, 663–668.
Sherman, J.D., 1996. Chlorpyrifos (Dursban)-associated birth defects: report of four cases. Arch. Environ. Health 51, 5–8.
Shih, T.M., et al., 2010a. In vivo reactivation by oximes of inhibited blood, brain and peripheral tissue cholinesterase activity following exposure to nerve agents in guinea pigs. Chem. Biol. Interact. 187, 207–214.
Shih, T.M., et al., 2010b. Treatment with tertiary oximes prevents seizures and improves survival following sarin intoxication. J. Mol. Neurosci. 40, 63–69.
Shinotoh, H., et al., 2004. Acetylcholinesterase imaging: its use in therapy evaluation and drug design. Curr. Pharm. Des. 10, 1505–1517.
Sidell, F.R., Groff, W.A., 1974. The reactivatibility of cholinesterase inhibited by VX and sarin in man. Toxicol. Appl. Pharmacol. 27, 241–252.
Sit, R.K., et al., 2011. New structural scaffolds for centrally acting oxime reactivators of phosphylated cholinesterases. J. Biol. Chem. 286, 19422–19430.
Sit, R.K., et al., 2014. Imidazole aldoximes effective in assisting butyrylcholinesterase catalysis of organophosphate detoxification. J. Med. Chem. 57, 1378–1389.
Skovira, J.W., et al., 2010. Protection against sarin-induced seizures in rats by direct brain microinjection of scopolamine, midazolam or MK-801. J. Mol. Neurosci. 40, 56–62.
Stephens, R., et al., 1995. Neuropsychological effects of long-term exposure to organophosphates in sheep dip. Lancet 345, 1135–1139.
Stine, K., Brown, T.M., 1996. Principles of Toxicology. CRC Lewis Publishers, Boca Raton.
Suganthi, M., Elango, K.P., 2017. Binding of organophosphate insecticides with serum albumin: multispectroscopic and molecular modelling investigations. Phys. Chem. Liq. 55, 165–178.
Sultatos, L.G., 1994. Mammalian toxicology of organophosphorus pesticides. J. Toxicol. Environ. Health 43, 271–289.
Tarhoni, M.H., et al., 2008. Albumin binding as a potential biomarker of exposure to moderately low levels of organophosphorus pesticides. Biomarkers 13, 343–363.
Tavitian, B., et al., 1993. In vivo visualization of acetylcholinesterase with positron emission tomography. Neuroreport 4, 535–538.
Taylor, P., 2018. Anticholinesterase Agents. McGraw-Hill Education, New York.
Viragh, C., et al., 1999. Small molecular products of dealkylation in soman-inhibited electric eel acetylcholinesterase. Biochemistry 38, 9557–9561.
Volkow, N.D., et al., 2001. Imaging brain cholinergic activity with positron emission tomography: its role in the evaluation of cholinergic treatments in Alzheimer's dementia. Biol. Psychiatry 49, 211–220.
Walker, W.F.H., Dominique, G., 1997. Anatomy and Dissection of the Rat. Freeman, W. H. & Company, New York.
Wallace, K.B., Herzberg, U., 1988. Reactivation and aging of phosphorylated brain acetylcholinesterase from fish and rodents. Toxicol. Appl. Pharmacol. 92, 307–314.
Welling, P.G., 1995. Differences between pharmacokinetics and toxicokinetics. Toxicol. Pathol. 23, 143–147.
Wilson, B.W., et al., 1992. Reactivation of organophosphorus inhibited AChE with oximes. In: Chambers, J.E., Levi, P.E. (Eds.), Organophosphates: Chemistry, Fate, and Effects. Academic Press, Inc., San Diego, pp. 107–137.
Worek, F., et al., 2008. Inhibition, reactivation and aging kinetics of highly toxic organophosphorus compounds: pig versus minipig acetylcholinesterase. Toxicology 244, 35–41.
Zhuang, Q., et al., 2018. Demonstration of in vitro resurrection of aged acetylcholinesterase after exposure to organophosphorus chemical nerve agents. J. Med. Chem. 61, 7034–7042.